

4. PHOTOGRAPH MATCHING TECHNIQUES AND DEMOGRAPHIC MODELS

4.1 OVERVIEW

The use of photo-identification techniques are a central part of our studies of the ecology of whale sharks. At Ningaloo, our photographic libraries date back to 1992 and have recently expanded with access to images provided by the ecotourism industry via the Western Australian Department of Environment and Conservation. With large databases, some form of automatic comparison of images using computer software is essential. This has recently become possible using the open-access, image matching software I³S. However, before the software can be routinely applied some knowledge of accuracy, precision and limitations of matching is required. These issues were addressed using the Ningaloo photo-identification database. We developed an information criterion (IC) algorithm that resulted in a parsimonious ranking of potential matches of individuals in an image library. Automated matches were compared to manual-matching results to test the performance of the software and algorithm. Validation of matched and non-matched images provided a threshold IC weight (approximately 0.2) below which match certainty was not assured. Most images tested were assigned correctly; however, scores for the by-eye comparison were lower than expected, possibly due to the low sample size. The effect of increasing horizontal angle of sharks in images reduced matching likelihood considerably. There was a negative linear relationship between the number of matching spot pairs and matching score, but this relationship disappeared when using the IC algorithm. The software and use of easily applied information-theoretic scores of match parsimony provide a reliable and freely available method for individual identification of whale sharks, with wide applications and the potential to improve mark-recapture studies without resorting to invasive marking techniques.

Given that we had an automated matching technique, we could use this software and our photo-identification library to examine demographic patterns. Precise estimates of demographic rates are key components of population models used to predict the effects of stochastic environmental processes, harvest scenarios and extinction probability. We used the 12-year photographic identification library of whale sharks from Ningaloo Reef to construct Cormack-Jolly-Seber (CJS) estimates of survival within a capture-mark-recapture (CMR) framework. Estimated survival rates, population structure and assumptions regarding age at maturity, longevity and reproduction frequency were combined in a series of age-classified Leslie matrices to infer the potential population trajectory of the population. Using data from 111 individuals, there was evidence for time variation in apparent survival (ϕ) and recapture probability (p). The null model gave a $\hat{\phi}$ of 0.825 (95% CI: 0.727 – 0.893) and $\hat{p} = 0.184$ (95% CI: 0.121 – 0.271). The model-

averaged annual $\hat{\phi}$ ranged from 0.737 to 0.890. There was little evidence for a sex effect on survival. Using standardized total length as a covariate in the CMR models indicated a size bias in ϕ . Ignoring the effects of time, a 5 m shark has a $\hat{\phi} = 0.59$ and a 9 m shark has $\hat{\phi} = 0.81$. Of the 16 model combinations considered, 10 (63%) indicated a decreasing population ($\lambda < 1$). For models based on age at first reproduction (α) of 13 years, the mean age of reproducing females at the stable age distribution (\bar{A}) ranged from 15 to 23 years, which increased to 29 to 37 years when α was assumed to be 25. All model scenarios had higher total elasticities for non-reproductive female survival ($E(s_{nr})$) compared to that for reproductive female survival ($E(s_r)$). Assuming relatively slow vital rates ($\alpha = 25$ and biennial reproduction) and size-biased survival probabilities suggest the Ningaloo Reef population of whale sharks is declining, although more reproductive data are needed to confirm this conclusion. Our work shows that combining relatively precise survival estimates from CMR studies with realistic assumptions of other vital rates provides a useful heuristic framework for determining the vulnerability of large oceanic predators for which little direct data exist.

Given modelled and observed (see Chapter 4) declines in whale shark numbers we interrogated the photo-identification data bases focusing on potential threats to this species. We recorded scars on whale sharks in three Indian Ocean aggregations (Australia, Seychelles and Mozambique), and examined whether scarring (mostly attributed to boat strikes and predator attacks) influences apparent survival rates using these photo-identification libraries. Scarring was most prevalent in the Seychelles aggregation (67 % of individuals). Predator bites were the most frequent source of scarring (aside from minor nicks and abrasions) and 27 % of individuals had scars consistent with predator attacks. A similar proportion of sharks had blunt trauma, laceration and amputation scars, the majority of which appeared to be caused by ship strike. Predator bites were more common (44 % of individuals) and scars from ship collisions were less common at Ningaloo Reef than at the other two locations. In all aggregations, scars occurred most often on the caudal fin, which may result from the fin being the body part closest to the surface when boats pass over or as a large target for predators. We found no evidence for an effect of scarring on apparent survival (ϕ) for the Ningaloo (not scarred $\phi = 0.858 \pm 0.033$; scarred $\phi = 0.929 \pm 0.033$) or Seychelles populations (not scarred $\phi = 0.502 \pm 0.060$; scarred $\phi = 0.538 \pm 0.070$). The lower apparent survival of the Seychelles population may be attributed to a high number of transient sharks in this aggregation that might bias estimates. We conclude that while scarring from natural predators and smaller vessels appears to be unrelated to whale shark survival, the effects of deaths related to ship strike need to be quantified to assist in future management of this species.

Ongoing work aims to quantify the extent of interchange among three major whale shark aggregations, Ningaloo Reef in Australia and Tofo Beach in Mozambique and Mahe Island, Seychelles. Ningaloo Reef and Tofo Beach are approximately 7,900 km apart, representing the eastern- and western-most extent of the distribution of whale sharks within the Indian Ocean, respectively, providing the best possible opportunity for differentiating putative stocks in

whale sharks on a regional scale. This study will be the first major photographic database comparison of whale shark aggregation sites.

4.2 VALIDATION OF COMPUTER-AIDED MATCHING

4.2.1 Introduction

As previously outlined in Chapter 3, photo-identification is being used to identify individuals in the whale shark population at Ningaloo Reef, Western Australia. This method also allows the collection of additional information to assist in estimating demographic parameters. The aim of this section is to validate computer-aided matching of individual whale sharks. The results from trials of the pattern-matching software and an information-theoretic validation technique will also be presented. Finally, the results from population size estimates based on the computer matched and validated images are presented.

4.2.2 Methods

4.2.2.1 Matching software, fingerprint creation and image matching

Prior to 2006, images of whale sharks were matched manually (by eye) in order to establish resights and population estimates (Meekan et al. 2006). As mentioned in Chapter 2, the software currently employed for matching photographs of whale sharks is Interactive Individual Identification System (I³S). This software, originally designed to match natural variation in spot patterns of grey nurse sharks (*Carcharias taurus*), was used to create 'fingerprint' files and match individuals. Fingerprint files are used to identify individual whale sharks based on their spot pattern, in a fashion analogous to the concept of human fingerprint recognition. The area on the flank of sharks directly behind the 5th gill slit was selected as the most appropriate area to use for identification of whale sharks. This area was chosen based on consistency with past studies, and due to the ease that photographers can focus on this area (Arzoumanian et al. 2005, Meekan et al. 2006). The positioning of spots in this area was also less likely to be distorted due to undulation of the caudal fin, which may affect the matching success of I³S.

The initial procedure once an image was entered into the database was to create a fingerprint file. Three reference points were required by I³S, points that could be easily and unambiguously identified in each photo were chosen: 1) the top of the 5th gill slit, 2) the point on the flank corresponding to the posterior point of the pectoral fin and 3) the bottom of the 5th gill slit (Figure 4.1).

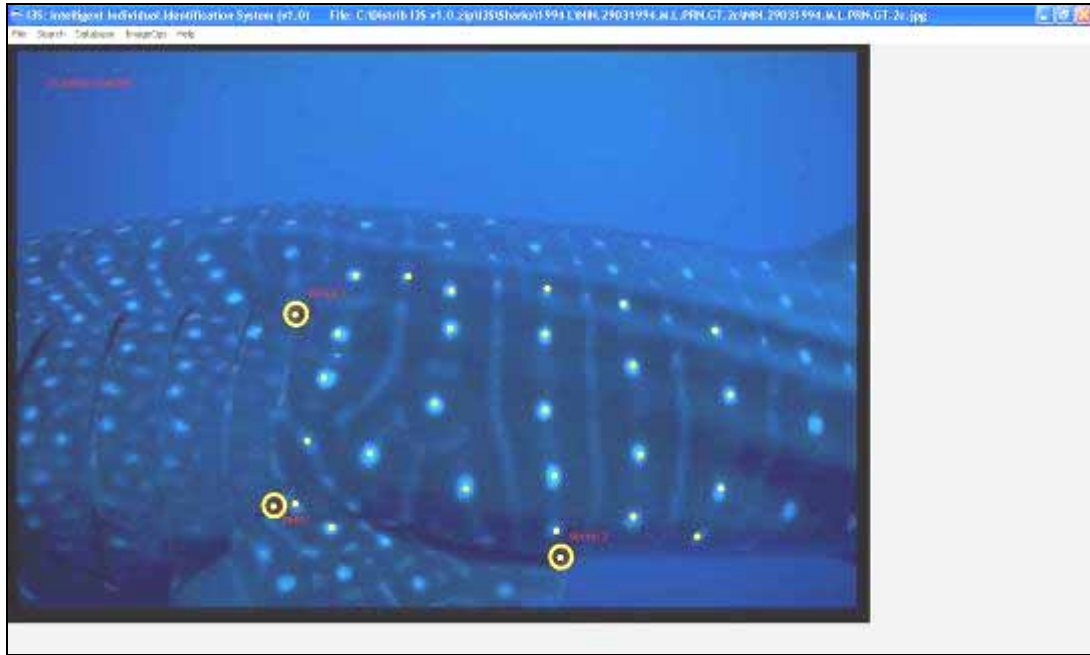


Figure 4.1. Fingerprint file creation (reference points and spot highlighting shown).

After the initial reference points for each image were entered, the centres of the most obvious spots within and slightly posterior to the reference area were highlighted by the operator. The reference area includes the spots behind the 5th gill slit, below the uppermost longitudinal ridge, and in front of the start of the dorsal fin. I³S requires a minimum of 12 spots to be highlighted to form a fingerprint, and a maximum of 40 spots. Highlighting spots outside of the immediate reference area can affect the ability of the I³S matching algorithm Van Tienhoven et al. 2007a; therefore, highlighted spots were kept roughly within the reference area for fingerprinting.

The requirement of all three reference points to be visible in the photograph for a fingerprint to be created meant that not all 797 photos in our database could be used. As such, 433 (54 %) of the original photographs could be used, of which 212 were of the left side (LS) and 221 were of the right side (RS) of the shark. To compare fingerprints, a common reference system is required, which is achieved by using a two-dimensional affine transformation Van Tienhoven et al. 2007a.

The transformation is calculated as follows:

$$M \begin{pmatrix} x \\ y \end{pmatrix} = \begin{pmatrix} m_{11} & m_{21} \\ m_{12} & m_{22} \end{pmatrix} \begin{pmatrix} x \\ y \end{pmatrix} + \begin{pmatrix} t_1 \\ t_2 \end{pmatrix} = \begin{pmatrix} m_{11}x + m_{21}y + t_1 \\ m_{12}x + m_{22}y + t_2 \end{pmatrix} \quad \text{Equation 1}$$

where M is the affine transformation matrix of x and y , and m_{11} , m_{21} , m_{12} , m_{22} , t_1 and t_2 are unknown variables (Van Tienhoven et al. 2007b).

The search function in I³S compares the new fingerprint file against all of the other fingerprint files in the database by using a two-dimensional linear

algorithm. The algorithm calculates the sum of the distances between spot pairs divided by the square of the number of spot pairs (Hartog & Reijns 2004). The matching algorithm is calculated as follows:

$$\frac{\sum d}{n^2} \quad \text{Equation 2}$$

Where d is the distance between matching spot pairs and n is the number of matching spot pairs. The matched spot pairs with the minimum overall sum of the squared distances between them is the most likely match, and given a score from 1 to 0 (0 being a perfect match). The program also lists the next 49 most likely spot pair matches, which it ranks in decreasing order of likelihood (Figure 4.2). The next step is to look at the most likely match, which is ranked as the top of the list of 50 matches. I³S provides a visual match of the unknown image and the image with which it was matched (Figure 4.3). A visual display of the matching spot pairs called a 'spot cloud' is also available to assist in matching individuals (Figure 4.4).

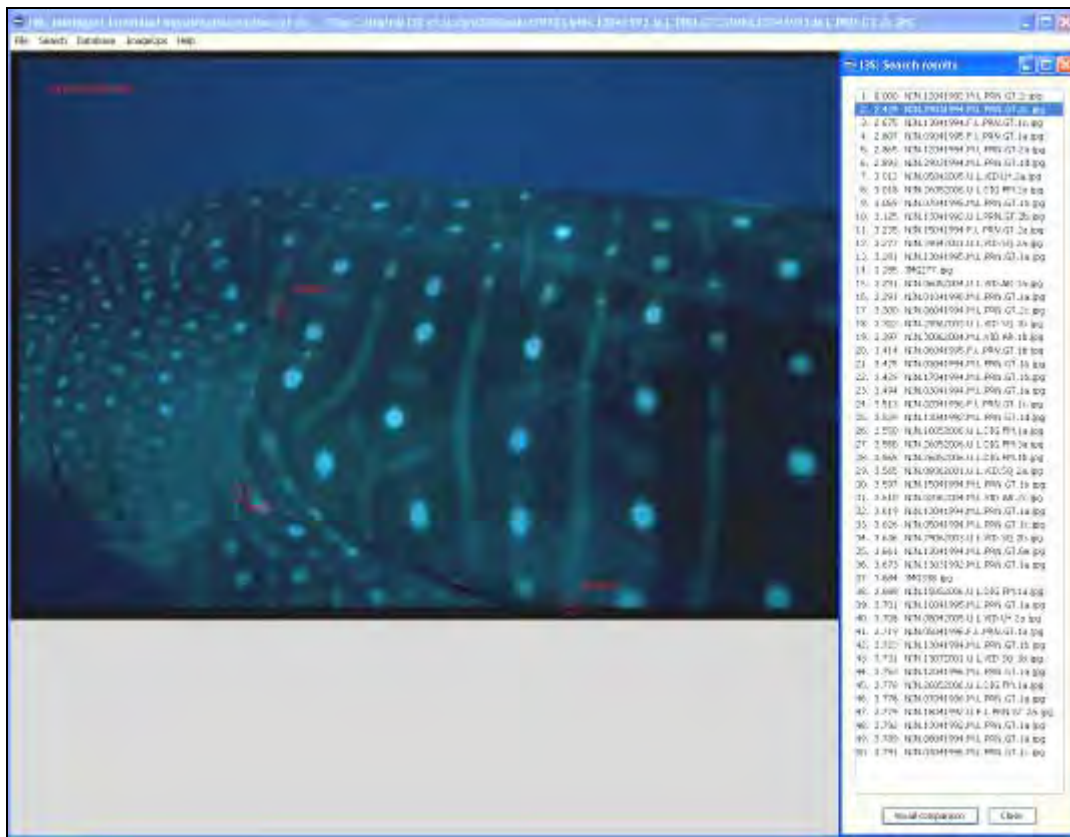


Figure 4.2. Results of searching an unknown image in I³S, showing unknown image and the top 50 ranking of the most likely matches (right side of the screen). Note. Because this example image was already present in the database, it was matched with itself (ranked number 1 in the list). Therefore, the image ranked in the second position is the most likely match in this situation.

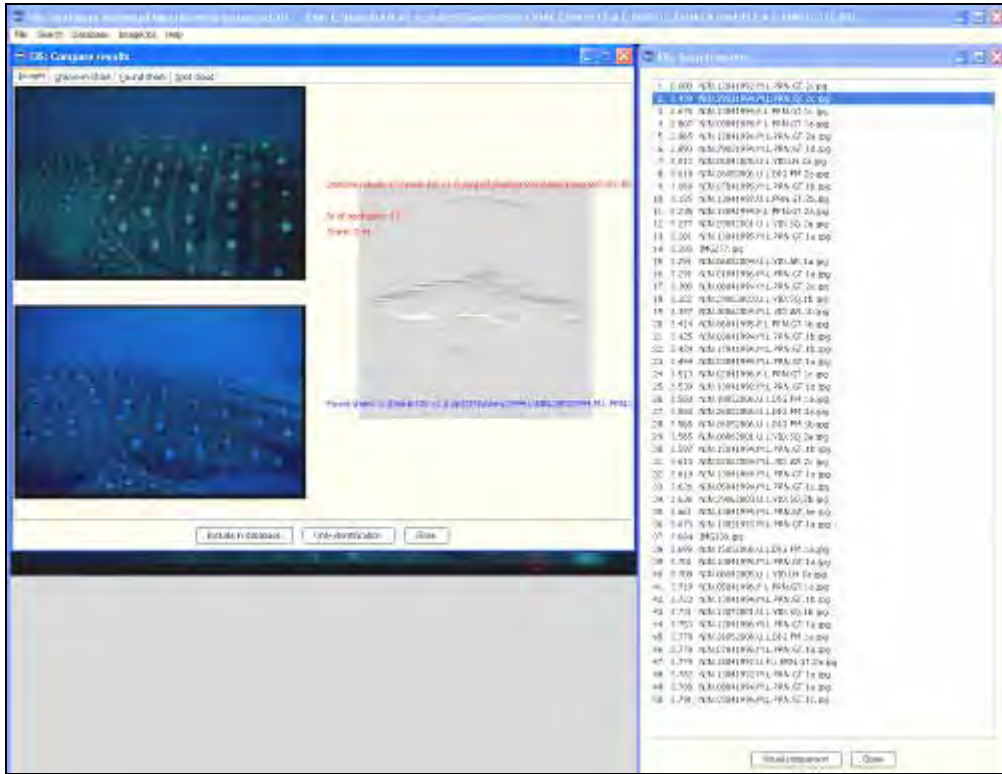


Figure 4.3. Visual comparison of unknown individual and matched individuals (left side of the screen). The top image is unknown, and the bottom image is the matched image from the database.

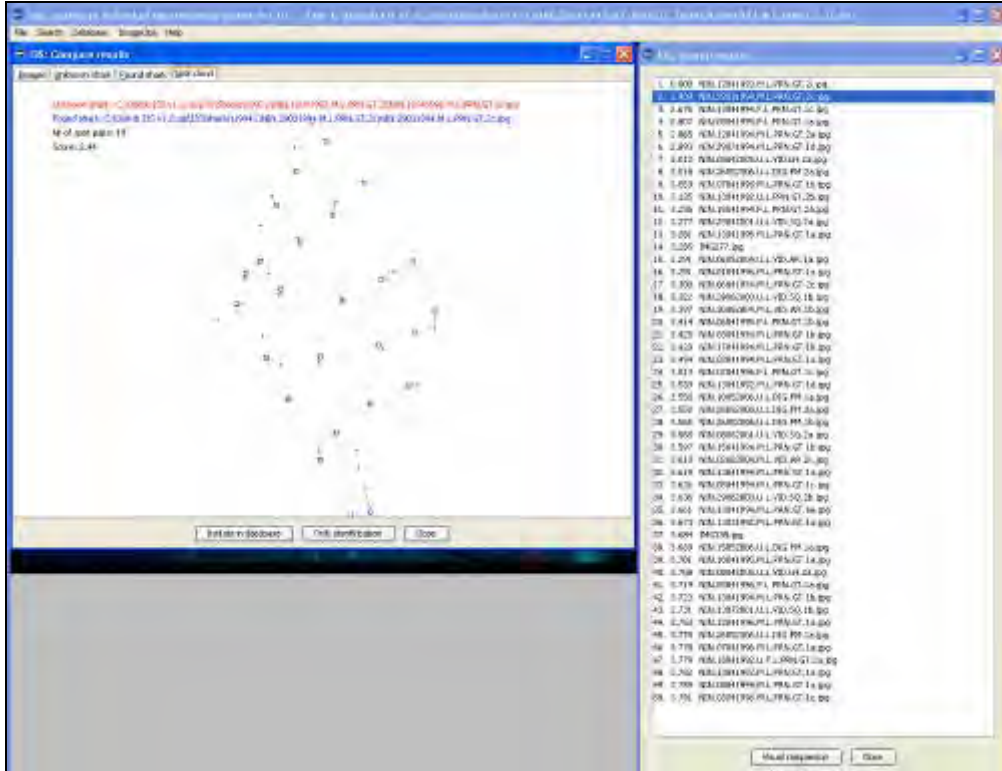


Figure 4.4. Spot cloud of matching spot pairs (left side of the screen). The red spots are the fingerprint from the unknown shark, and the blue spots are the fingerprint from a shark found in the database. The green lines denote the distance between match spot pairs.

4.2.2.2 I³S matching validation

I³S provides the user with a matching score (>0); however, this score does not take into account the uncertainty in the system, nor does it provide a relative score to all other images considered. A non-subjective validation technique is essential to assess the relative strength of matches, which has not been provided to date for automated photo-identification studies. Without a validation of image matches, the final decision is subjective, and may affect the quality of data used for parameterisation of demographic models.

To provide a measure of match parsimony based on the philosophy of information theory and to compare possible image matches in a multi-model inferential framework Burnham & Anderson 2002, the match score was modified in the following manner: (1) the spot-averaged sum of squares was back transformed to a residual sum of squares, which was simply the spot score (*SS*) multiplied by the square of the number of matching spots (*n*); (2) an information criterion (IC) analogous to the Akaike Information Criterion (Akaike 1973) or Bayesian Information Criterion (Link & Barker 2006) was developed as follows:

$$IC = 2k + n' \log_e \left(\frac{SS \cdot n^2}{n'} \right) \quad \text{Equation 3}$$

where *k* = an assumed number of parameters under a simple linear model (set to 1 for all models) and the $n' = 100/n$ and accounts for the fact that an increasing number of spots automatically leads to a higher *SS* (the 100 multiplier scales the term to be > 1);

(3) the IC weight (*w*) was calculated as:

$$w_i = \frac{e^{-0.5 \cdot \Delta IC_i}}{\sum_{i=1}^m \Delta IC_i} \quad \text{Equation 4}$$

where $\Delta IC = IC - IC_{min}$ for the *i*th image (*i*th 'model') 1 through *m* (where *m* = 49);

(4) finally, the evidence ratio (*ER*) was calculated as:

$$ER_1 = \frac{w_1}{w_2} \quad \text{Equation 5}$$

This IC algorithm was applied to a sample of 200 images; 25 matching pairs from the LS and RS databases and 25 non-matching pairs from the LS and RS

databases. The LS and RS images were analysed separately using text outputs from I³S showing image name, I³S matching score and number of pairs matched by I³S (Appendix 1). The analysis was done using the R Package (R Core Development Team 2004); the code for the IC algorithm, (including *w* and *ER*), is given in appendix 2.

4.2.2.3 Assessing 'by-eye' matches using I³S

Thirty-three sharks were re-sighted inter-annually during the manual 'by-eye' analysis of the raw photo library (Meekan et al. 2006). Of any two by-eye matched images, one of the pair was entered into either the LS or RS database and searched. A match using I³S was successful if the by-eye matched images were ranked as the most likely match (as with the validation test) and confirmed using the IC algorithm (i.e., $w_1 \geq 0.2$).

4.2.2.4 Horizontal angle (yaw)

Video footage of 10 different sharks (5 LS and 5 RS) was used to capture sequences of five images per shark, where subjects were on differing horizontal angles (0°, 10°, 20°, 30° and 40° – Figure 4.5). The angles of yaw were estimated using Screen Protractor™ software. Fingerprints were created for each image with 20 spots highlighted per fingerprint. The 10° images were searched against the 0° images and 10 non-matching images. This process was repeated, substituting images where subjects were on angles of 20°, 30° and 40° for both LS and RS image sequences. Five random, non-matching pairs were also searched against 0° and 10° images, and then repeated for 20°, 30°, and 40° images. This allowed for a comparison between matching and non-matching pairs while testing for the effects of horizontal angle in images. Results were analysed using the same IC algorithm applied to the match validation and by-eye comparison tests.



Figure 4.5. - An individual whale shark at differing angles of yaw (A: 0°, B: 10°, C: 20°, D: 30°, E 40°). This type of sequence was used to determine the effect of horizontal angle on the I³S matching process.

4.2.2.5 Number of spot pairs

Fifty known-matching pairs were compared to one another using I³S. Only the matching pairs that were successfully confirmed during validation of I³S matches were included in this test. I³S scores were compared against the number of spot pairs matched in I³S. The w_1 for each image was also compared against the number of spot pairs matched by the I³S algorithm. A complementary log-log transformation (clog-log) was applied to normalize the distribution of I³S scores and w_1 , and a \log_{10} transformation was used to normalize the distribution of spot pairs. We tested for a linear relationship

between the transformed variables using least-squares regression and information-theoretic evidence ratios. Goodness-of-fit was tested using the least-squares R^2 value.

4.2.2.6 Population Size Analysis

The initial population size estimates for this study were calculated using a capture matrix based on I³S matches. The capture matrix consisted of all individuals with both sides fingerprinted, and RS only fingerprinted. Individuals which had LS fingerprinted only, were excluded to reduce the potential error of double counting individuals. Only inter-annual sightings of individuals were included within the capture matrix. Population size estimates were further refined by repeating the experiment using the capture matrix consisting of only I³S matches that had been validated using the IC algorithm. Images that received IC w scores above the IC w threshold were considered to be validated. All resights that were not validated were removed from the capture matrix prior to reanalysis. Similarly, this capture matrix only consisted of inter-annual sightings of individuals.

Population estimates using a series of closed population models (assuming no net immigration or emigration) were initially calculated using the program CAPTURE, and examined variants of the Lincoln-Petersen (LP) model (Meekan et al. 2006). Due to the sensitivity LP estimates to temporary emigration and the low power associated with databases comprising a low rate of recapture (resighting), an open-population Cormack-Jolly-Seber model (Schwarz & Arnason 1996) was also applied using the POPAN option in the program MARK (White & Burnham 1999) to estimate population abundance (Table 4.1).

Table 4.1. Open-population models for whale shark population re-assessment using MARK

Model Name	Model Equation
<i>Constant (null)</i>	$\phi(\cdot)p(\cdot)\beta(\cdot)N(\cdot)$
<i>Capture probability-time variant</i>	$\phi(\cdot)p(t)\beta(\cdot)N(\cdot)$
<i>Apparent survival-time variant</i>	$\phi(t)p(\cdot)\beta(\cdot)N(\cdot)$
<i>Probability of entry-time variant</i>	$\phi(\cdot)p(\cdot)\beta(t)N(\cdot)$

Note: ϕ = apparent survival, p = capture probability, β = probability of entry to population per occasion and N = super-population size.

Time intervals were set according to years sampled between 1992 and 2006 which were yearly from 1992-1996, 2001, then again yearly from 2003-2006). As such, the number of years elapsed between resighting events (years) was 1, 1, 1, 1, 5, 2, 1, 1 and 1. All models were fitted using the logit link function for ϕ and p , the identity link function for N , and the multinomial logit link function (MLogit [1]) to constrain the β parameters to be ≤ 1 (White & Burnham 1999). Parameters counts (k) for each model were adjusted to account for the fact that not all were estimable due to low recovery rates in some years. Akaike's Information Criterion corrected for small sample sizes (AIC_c) was adopted to

give a model comparison and model-averaged estimates of N (Burnham & Anderson 2002). AIC_c was calculated as follows:

$$AIC_c = -2\log L + 2k + \frac{2k(k+1)}{n-k-1} \quad \text{Equation 6}$$

Goodness-of-fit was calculated using the program RELEASE implemented in MARK. The coefficient of variation (CV) was also calculated for each model as a measure of parameter precision for abundance estimates:

$$CV = \frac{Sd}{\bar{x}} \times 100 \quad \text{Equation 7}$$

4.2.3 Results

4.2.3.1 I³S (Interactive Individual Identification Software) matching validation

The Information Criterion weights (w_1) for the most parsimonious matches (w_1) for the 50 matched pairs were broadly distributed between 0.05 and 0.85, while w_1 for non-matched pairs were highly right-skewed (Fig. 4.6a,b). All w_1 for non-matched pairs were < 0.18 . The median w_1 for matched pairs was $0.32 (\pm SE 0.05)$, which was much greater than the median for non-matched pairs (0.06 ± 0.01). Evidence ratios for the best-matched relative to the next-highest matched images (ER_1) for known matched pairs were also highly right-skewed and ranged from 0.73 to 51.92, with a median of $7.36 (\pm 2.45)$ (Fig. 4.6c). ER_1 values for non-matched pairs were all < 3.5 (median = 1.21 ± 0.09) (Fig. 4.6d). Evidence ratios for the second best-matched relative to the next-highest matched images (ER_2) for known matched pairs ranged from 0.73 to 114.18, with a median of $7.57 (\pm 3.82)$. ER_2 values for non-matched pairs were also all < 3.5 (median = 1.42 ± 0.12).

Overall, 93 images out of the 50 known-matched pairs were matched correctly using I³S. w_1 for the correctly assigned matches ranged from 0.05 to 0.85 (median = 0.36 ± 0.05), and their ER_1 ranged from 0.73 to 51.92 (median = 8.82 ± 2.56) (Figure 4.7 a & b). Known-matched photographs that I³S failed to match (7 images) had w_1 that ranged from 0.05 to 0.14 (median = 0.07 ± 0.02), with their ER_1 ranging from 0.95 to 2.28 (median = 1.23 ± 0.36).

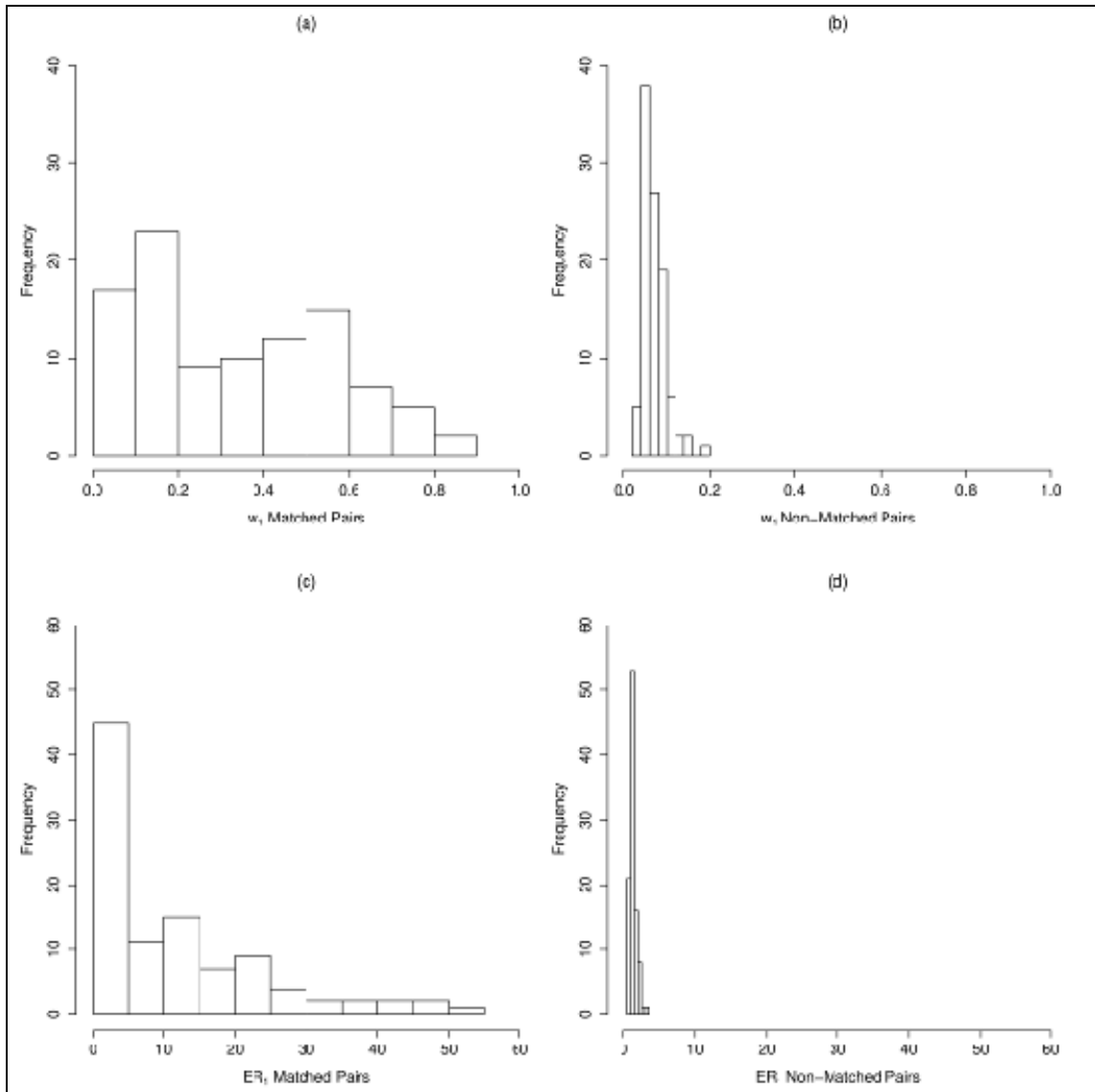


Figure 4.6. I³S matching validation IC weights (w_1). Distribution of IC weights for known matched (a) and non-matched pairs (b), and I³S matching validation evidence ratios (ER_1) for known matched (c) and non-matched pairs (d) are shown.

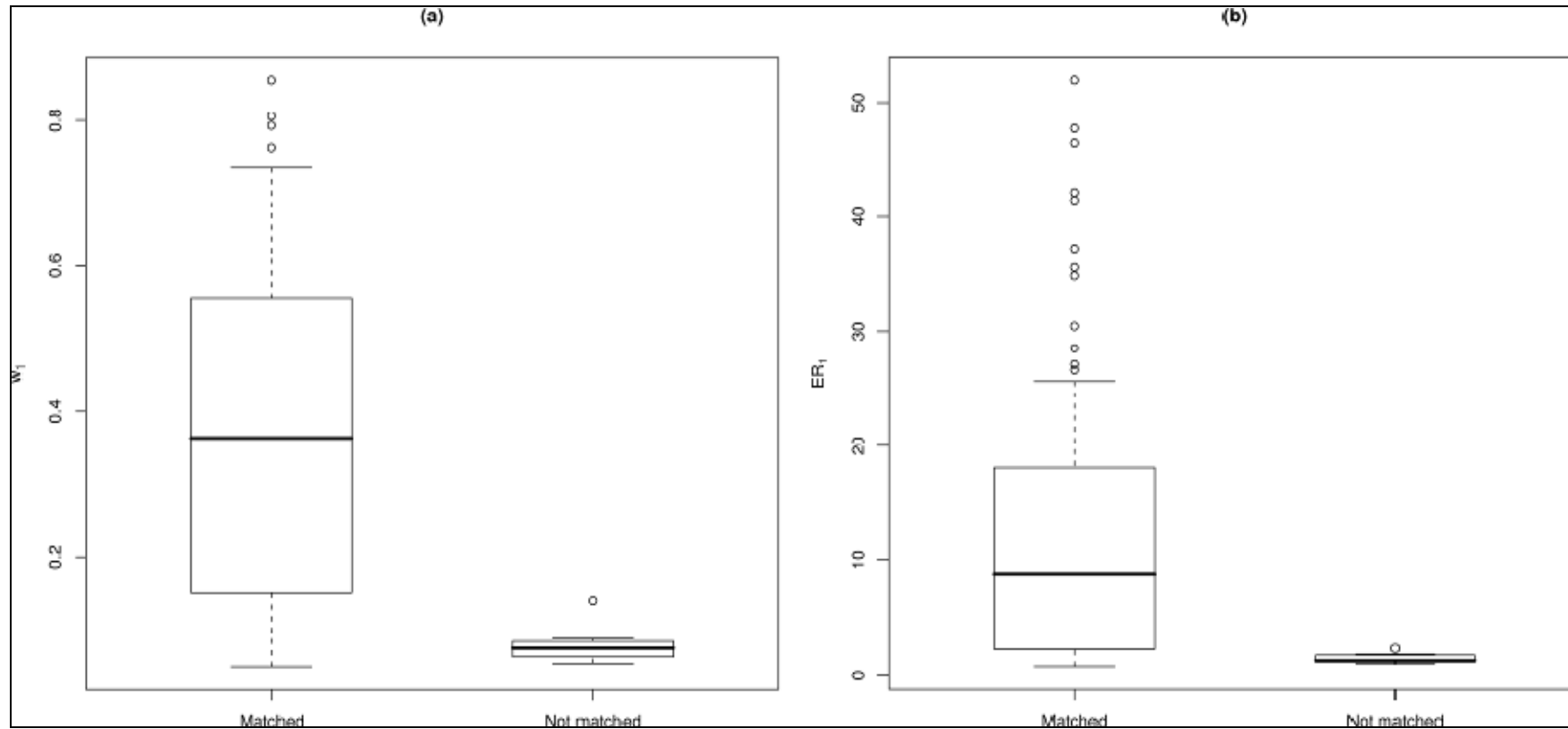


Figure 4.7. Median (a) IC weights (w_1) for known matched pairs showing images matched and not matched with I³S; (b) Median evidence ratios (ER_1) for known matched pairs showing images matched and not matched using I³S.

4.2.3.2 Assessing 'by-eye' matching using I³S

Ten of the 33 individuals re-sighted between years in the database used by Meekan et al. (Meekan et al. 2006) could not be matched with I³S because their images were not amenable to I³S fingerprinting (absence of reference points), or their match was not present in the database. This was because the Meekan et al. (2006) study also used images from a separate database and included scar-identified individuals that were not available for photographic matching using I³S. Therefore, we could only re-assess 23 of these by-eye matches that included 13 LS matches and 16 RS matches (58 images total).

Forty-eight of the 58 images (83 %) from the 23 individuals were matched correctly using I³S. w_1 for the correctly assigned by-eye matches ranged from 0.05 to 0.53 (median = 0.16 ± 0.04) (Fig. 4.8a), and their ER_1 were between 1.04 and 24.57 (median = 2.33 ± 1.58) (Fig. 4.8b). Incorrectly assigned by-eye matches had w_1 ranging from 0.04 to 0.13 (median = 0.06 ± 0.01) and their ER_1 ranged from 0.67 to 2.76 (median = 1.04 ± 0.37). I³S also identified two images that were false positives (i.e. sharks that were incorrectly matched with other photographs) in the by-eye matching process. Neither of these images was matched with other known images of the identified sharks.

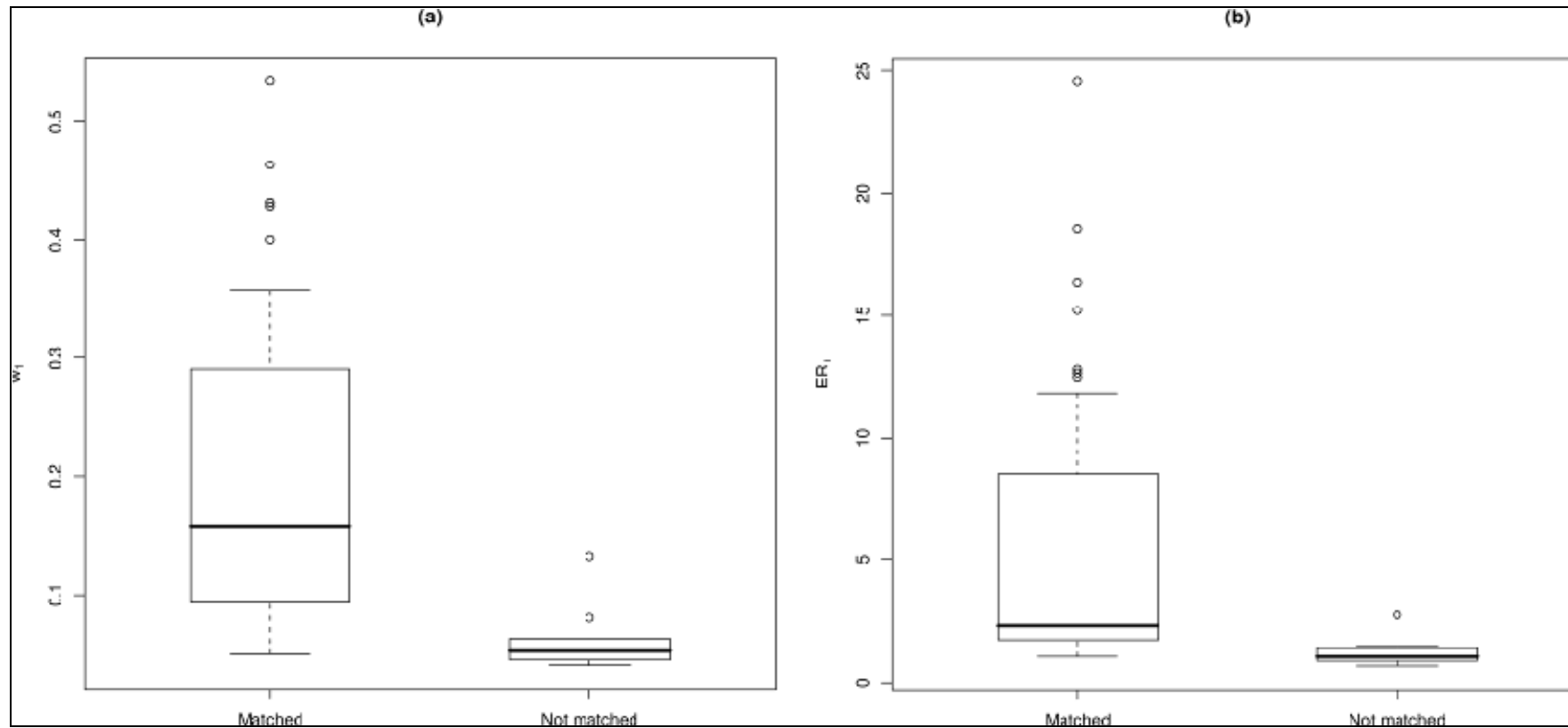


Figure 4.8. By-eye versus I3S matching Results. (a) Median IC weights (w_1) for by-eye matched images that were matched and not matched using I3S; (b) Median evidence ratios (ER_1) for by-eye matched images that were matched and not matched using I3S.

4.2.3.3 Horizontal angle

Mean w_1 scores decreased linearly as the horizontal angle of subjects within images increased (Figure 4.9 a). Mean w_1 scores ranged between 0.88 (± 0.06) for angles of 10° , to 0.30 (± 0.13) for angles of 40° . Standard errors for w_1 were relatively low for angles of 10° and 20° ; however, these increased noticeably for angles of 30° and 40° . The images of subjects at 30° approached mean w_1 scores for non-matching pairs, and mean w_1 scores for images of subjects at 40° overlapped mean w_1 scores for non-matching pairs.

There was an exponential decline of mean ER_1 with increasing angle (Figure 4.9b). Mean ER_1 ranged from 89.42 (± 52.23) for images of subjects at 10° to 4.06 (± 2.80) for images of subjects at 40° . The images of subjects at 30° approached mean ER_1 for non-matching pairs, and mean ER_1 for images of subjects at 40° overlapped mean ER_1 for non-matching pairs.

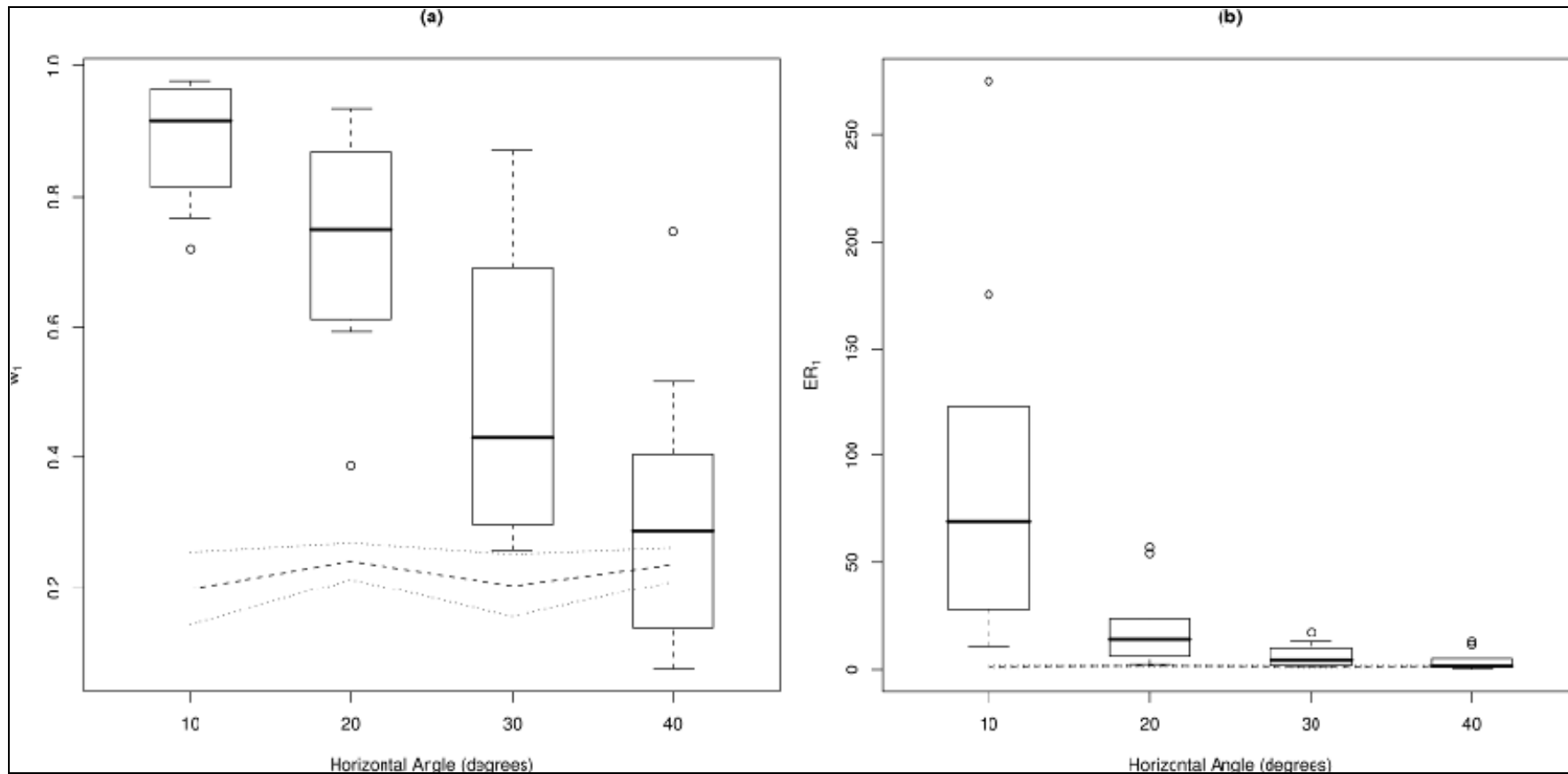


Figure 4.9. Effect of angles of yaw. (a) Mean IC weights (w_1) for horizontal angle categories, where images at 0° were matched against images skewed by 10°, 20°, 30° and 40°. Dotted lines show results for non-matching pairs; (b) Mean evidence ratios (ER_1) for horizontal angle categories, where images at 0° were matched against images skewed by 10°, 20°, 30° and 40°.

4.2.3.4 Number of spot pairs

There was evidence for a negative relationship between the transformed $\delta^{13}\text{S}$ scores and spot pairs ($ER = 9.94 \times 10^5$, adjusted $R^2 = 0.26$; Figure 4.10 a), but no evidence for a relationship between transformed w_1 and the number of spot pairs ($ER < 1$; Figure 4.10 b).

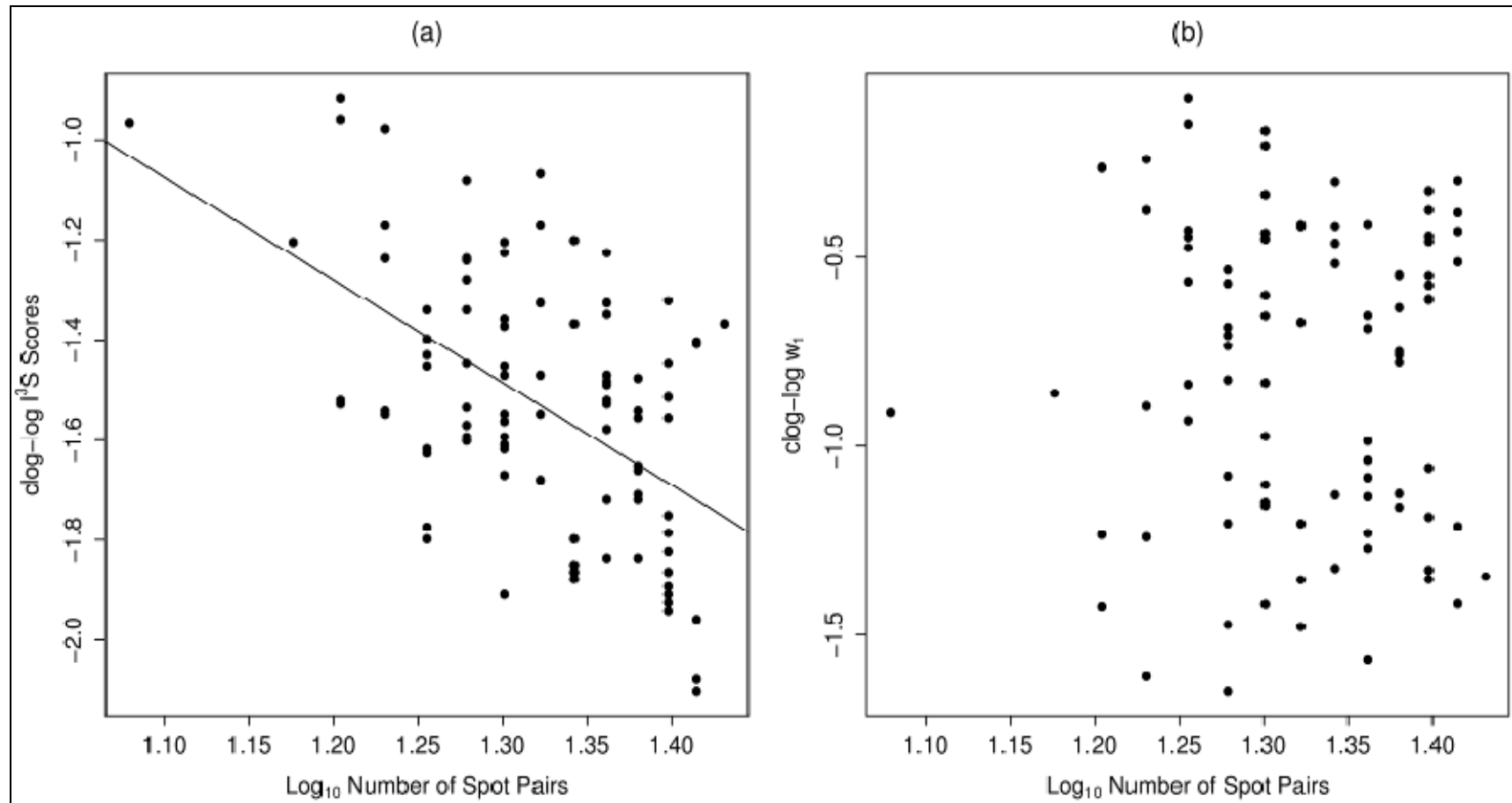


Figure 4.10. Effects of spot-pair number. (a) Relationship between complementary log-log-transformed (clog-log) I³S scores and log₁₀-transformed number of spot pairs. The fitted line illustrates the correlation observed using a linear regression; (b) Comparison of clog-log-transformed w₁ with log₁₀-transformed number of spot pairs.

4.2.3.5 Whale shark population size using I³S matches

After the removal of multiple images of the same individual, a total number of 208 individual sharks were identified for the period between 1992 and 2006 (excluding 1997, 1998, 1999, 2000 and 2002). Eighty-four of these individuals had both RS and LS fingerprints, 73 had RS fingerprints only and 51 had LS fingerprints only. We therefore excluded individuals with LS only fingerprints to avoid double counting the same individual, which left a total of 157 individuals suitable for use in population estimates. From a total of 157 individuals, there were 30 individuals that were resighted inter-annually. Twenty-six of these were included in the population analysis because they either had the right side or both sides fingerprinted.

Ten capture sessions (excluding years where sampling did not occur) including 157 individuals with fingerprints, seen in 187 separate sightings over the study period, enabled the estimation of population size using differing models and estimators. The model that provided the best fit under the model selection criteria provided by CAPTURE was the time-variant and heterogeneity model (M_{th} , model selection criterion = 1.0). Tests for closure ($z = -1.886$, $P = 0.029$) and closure by frequency of capture ($z = -3.825$, $P = 0.00007$) both violated the assumption of homogeneity of capture probabilities (i.e., the population was not closed). The M_{th} model using the Chao estimator provided time-variant capture probabilities (p_i) ranging between 0.01 (2005) and 0.08 (1994). No trend was observed over time. Population estimates are summarised in (Table 4.2).

Table 4.2. Summary of population size estimates from closed and open populations for I³S resights

Model		Goodness of Fit	N Range	CV (%)
<u>Closed</u>				
M_{th} (1992-2006)			367-780	20
M_{tb} (1992-2006)	Chao	$\chi^2_7 = 34.64$ $P = <0.001$	189-5216	150
M_t	Chao	$\chi^2_{58} = 71.95$ $P = 0.102$	347-628	15.5
<u>Open</u> (Jolly Seber)				
$\phi(\cdot)p(\cdot)\beta(\cdot)N(\cdot)$		$\chi^2_1 = 0.28$ $P = 0.60$	265-363	8.2
$\phi(\cdot)p(\cdot)\beta(t)N(\cdot)$		$\chi^2_1 = 0.28$ $P = 0.60$	265-363	8.2

Note: ϕ = apparent survival, p = capture probability, β = probability of entry to population per occasion and N = super-population size.

Only one of the parameters for time-variant models converged using the POPAN open-population Jolly-Seber model structure, which was the time-variant probability of entry model ($\phi(.)p(.)\beta(t)N(.)$). The reason that many of the time variant models did not converge was due to some parameters being inestimable from a low number of resights in particular years. The constant model ($\phi(.)p(.)\beta(.)N(.)$) converged with an AIC_c of approximately 100 % (Table 4.3) and provided a super-population size of 265-363 individuals (Table 4.2).

Table 4.3. Results for model analysis using non-validated (unvalidated) I³S dataset - Small sample size corrected Akaike Information Criterion (AIC_c), change in AIC_c (ΔAIC_c), AIC_c weights (w_{AIC_c}), number of parameters (k) and deviance.

Model	AIC_c	ΔAIC_c	w_{AIC_c}	NP (k)	deviance
$\phi(.)p(.)\beta(.)N(.)$ 1	16252.949	0.0000	0.99841	3	15420.6390
$\phi(.)p(.)\beta(t)N(.)$	16265	12.8868	0.00159	9	15420.6390

4.2.3.6 Whale shark population size using validated I³S matches

Using the w_i threshold of 0.2 determined from the validation tests, only 14 of the 26 individuals resighted inter-annually were validated. w_1 for validated resights ranged between 0.21 and 0.77, with a mean of 0.41 (S.E \pm 0.08) (Figure 4.11). w_1 for non-validated (unvalidated) resights ranged between 0.05 and 0.14, with a mean of 0.06 (S.E \pm 0.02).

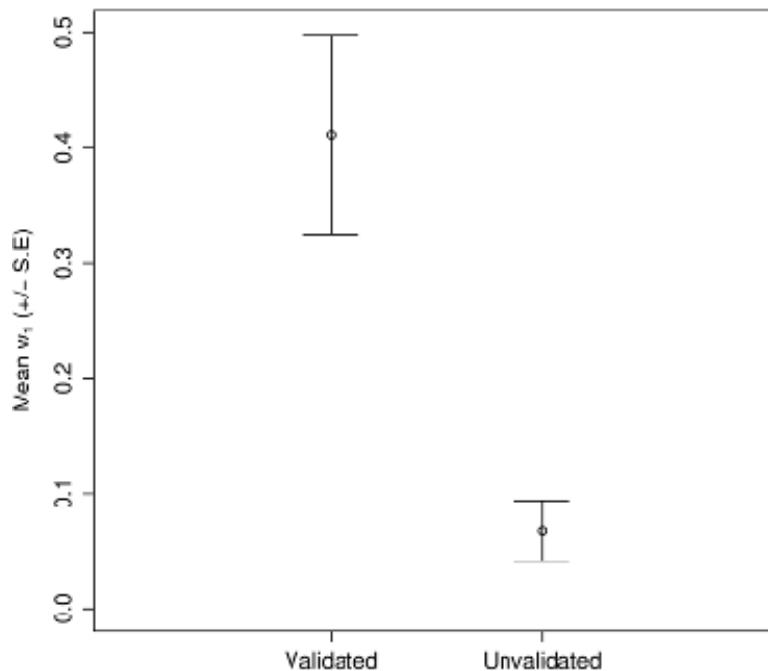


Figure 4.11. Mean validated and unvalidated (< 0.2) w_1 for inter-annual resights used for population modelling.

The ten capture sessions included 145 individuals with fingerprints seen in 161 separate sightings over the study period. These were used to create IC-validated population estimates using differing models and estimators. The model which provided the best fit under the model selection criteria provided by CAPTURE, was the time variant model (M_t) ($\chi^2_{56} = 58$, $P = 0.40$, model selection criterion = 1.0) (Table 4.4).

The test for closure ($z = -2.783$, $P = 0.002$) and closure by frequency ($z = -3.525$, $P = 0.00021$) were both violated under the null model of no heterogeneity in capture probabilities. The M_t model using the Chao estimator provided time-variant capture probabilities (p_t) ranging between 0.01 (1993) and 0.05 (1994). No trend was observed over time. Population estimates are summarised in Table 4.4.

The only time-variant model with converging parameters was the time-variant probability of entry model. The constant model using the POPAN open-population Jolly-Seber model structure implemented in MARK for 1992-2004 estimated the super-population size at between 280 and 452 individuals, with an AIC_c of approximately 90 % (Table 4.5).

Table 4.4. Summary of population size estimates from closed and open populations for validated I3S resights

Model		Goodness of Fit	N Range	CV (%)
Closed				
M_t (1992-2006)	Chao	$\chi^2_{56} = 58$ $P = 0.40$	447-1211	26.2
M_{tb} (1992-2006)	Chao	$\chi^2_7 = 27.74$ $P = < 0.001$	176-8696	203
M_{th} (1992-2006)			497-1428	28
Open (Jolly Seber)				
$\phi(.)p(.)\beta(.)N(.)$			280-453	12.4
$\phi(.)p(.)\beta(t)N(.)$			280-453	12.4

Table 4.5. Results for model analysis using validated I3S dataset - Small sample size corrected Akaike's Information Criterion (AIC_c), change in AIC_c (ΔAIC_c), AIC weights ($w AIC_c$), number of parameters (k) and deviance.

Model	AIC_c	ΔAIC_c	$w AIC_c$	NP (k)	deviance
$\phi(.)p(.)\beta(.)N(.)$	11517.486	0.0000	0.89255	3	10803.5630
	9				
$\phi(.)p(.)\beta(t)N(.)$	11521.721	4.2342	0.10745	5	10803.5630
	1				

4.2.4 Discussion

4.2.4.1 I³S Analysis & Information Criterion Algorithm

Our assessment of I³S, coupled with an incorporation of an information-theoretic algorithm was effective given that the natural spot pattern of whale sharks was well suited to this system. Validation of I³S matches using the Information Criterion algorithm provided a threshold w_1 for known matched pairs of approximately 0.2, below which w_1 for non-matched pairs fell. Known matched pairs not matched by I³S, or that were matched with low (i.e., < 0.2) w_1 , probably resulted due to poor clarity or high angles of yaw. This highlights the need to only select images of the highest quality for matching purposes (Friday et al. 2000). The validation process is necessary with most computer-aided matching algorithms because this alleviates much of the subjectivity associated with the final stage of matching

I³S (open access at www.reijns.com/i3s), was effective at confirming past matches made by eye in most instances. Images that were successfully confirmed using our Information Criterion algorithm received relatively low w_1 and ER_1 overall, most likely as a result of a considerably smaller sample size than that used for validation. I³S was also a useful tool for identifying image matches that were assigned incorrectly (i.e., both false positives and false negatives). When matching whale shark patterns by eye, the observer generally does not focus on the spots *per se*; rather, attention is usually paid to the lines and whirls (see Fig. 4.1) on the flank of the shark. I³S therefore provides an unbiased method of matching natural markings, which is relatively impervious to user subjectivity.

We found strong evidence that horizontal angle of subjects within images compromises the ability of the I³S algorithm to make reliable matches. As the horizontal angle of subjects in images increases, the matching likelihood decreases. Angles of yaw up to 30° compromise the matching process even though many of these images were still matched correctly. Conversely, images with angles of yaw $\geq 40^\circ$ will more than likely be incorrectly assigned. Due to the linear algorithm used by I³S to match spot patterns it is important to use only those photos with little or no contortion of the reference area. Likewise, the number of spots annotated in fingerprints can also potentially influence the I³S matching process. The higher the number of spot pairs matched, the lower the I³S score and hence, the higher the matching certainty. This corroborates similar findings from a study of *Carcharias taurus* (Van Tienhoven et al. 2007b) and emphasizes the benefit of using information-theoretic measures of matching parsimony because the updated algorithm takes relative match certainty into account.

The number of suitable images from our database for use in I³S was considerably reduced due to the absence of reference points, poor image quality and oblique angles of subjects. The rejection rate is inflated particularly by the use of photographs taken without the explicit aim of photographic matching because many are derived from ecotourism operations. However, the efficiency and reliability of matching with I³S more than compensated for

the reduced sample size. The number and size of images in an I³S database can potentially slow down the program's operating speed; therefore, it is ideal to scale down the size of photographs and only include the best image of a particular animal. In addition to horizontal angle, roll and pitch of sharks in images may affect the matching process. Pitch seems likely to be only a minor problem, because digital photos can be rotated so that the animal is aligned with the horizontal. We had few images of the same individual at varying angles of roll, so we were unable to examine this potential problem.

4.2.4.2 Estimating population size

The first population estimates for the aggregation of whale sharks at Ningaloo Reef were based on a dataset of images collected between 1992 and 2004, from which 184 individuals were identified manually (Meekan et al. 2006). Data from 2005 and 2006 were included in this analysis, in which an additional 24 individuals were identified (a total of 208 individuals). The first population estimates were based on 159 individuals, where either images for both sides or the right side were present (i.e., left side-only images were discarded to remove the possibility of double-counting individuals). There were a similar number of individuals (157) identified for population assessment in this study. Meekan et al. (2006) identified 33 individuals which were resighted between 1992 and 2004, which compared to 30 individuals identified by I³S in this study between 1992 and 2006. Despite the Meekan et al. (2006) study having fewer sampling occasions, fewer individuals were identifiable in this study due to a large number of images being incompatible for matching with I³S.

Population estimates based on data obtained via I³S matches were similar to the initial open population estimates found by Meekan et al. (Meekan et al. 2006) – the Ningaloo super-population (i.e. the population of individuals that visit Ningaloo Reef) is between 300 and 500 individuals based on open population models, with closed population estimates providing a much wider range (176-8696). This provides evidence to support the hypothesis that initial population estimates made by eye were a reasonable approximation. The relatively high number (12 of 26) of known inter-annual resights that were not validated using information criteria weights was most likely due to oblique horizontal angles of subjects in images found in the I³S validation tests (Fig.4.1). The resights that had information criteria weights below the pre-determined certainty threshold (0.2) were removed from the capture matrix prior to population re-analysis to remove any uncertainty in resights. The information criteria weights and evidence ratios provide a measure of match parsimony based on the strength of matches, which can be misleading if the quality of images compared are poor (see Friday et al. 2000). Therefore, rather than dismissing resights completely based on low information criteria weights or evidence ratios, it is more appropriate to make the final decision by manual inspection under these circumstances.

The use of validated images for population estimation has provided a measure of certainty in resights and resultant estimates of population parameters such as abundance and vital rates (e.g., survival and population trajectories; Bradshaw et al. 2007). The validation of image matches also assists in reducing

identification errors which are common in photo-identification, such as false-positives and false-negatives. These types of errors can greatly inflate population estimates (Stevick et al. 2001), which can have serious implications for the management of threatened populations. Population estimates for whale sharks at Ningaloo Reef are based on the assumption that their spot and stripe patterns remain stable through time. Therefore, if ontogenetic changes in spot patterns do occur, the number of individuals resighted will likely be underestimated and estimates of population size would be upwardly biased (Meekan et al. 2006).

In addition to data quality, sampling effort has the potential to affect estimates if it has varied over sampling periods. Sampling effort varied between the periods of 1992-2003 and 2004-2006 in this study. This variation in sampling effort may be a contributing factor to the few resights seen in recent years; nevertheless, population estimates should be viewed tentatively until enough image matches are obtained to reduce uncertainty (Meekan et al. 2006). Future estimates of population size should be facilitated by the recent policy of photo sharing implemented by the Western Australian Department of Environment and Conservation (DEC), described in Chapter 2.

4.3 MODELLING OF DEMOGRAPHY: INFERRING POPULATION TRENDS FOR THE WORLD'S LARGEST FISH FROM MARK-RECAPTURE ESTIMATES OF SURVIVAL

4.3.1 Introduction

Demographic data are useful for determining the effects of stochastic processes on abundance (Sibly & Hone 2002), the type and strength of regulation operating on a population (Bradshaw et al. 2005, Sibly et al. 2005), and extinction risk faced by populations under various environmental scenarios (Fagan & Holmes 2006). However, demographic data alone cannot always divulge the mechanisms responsible for population trajectories, which is especially inconvenient when management actions are required to mitigate decline (McMahon & Burton 2005). Population viability analyses (PVA) have provided a means to examine the relative contributions of competing factors on rates of population change (Cochran & Ellner 1992, Caswell et al. 1999), and have given useful heuristic direction in managing the processes threatening species of conservation concern (Brook & Bradshaw 2006). Despite this advance, most PVA models rely on detailed life history data (Ellner et al. 2002) and researchers are forced to make profligate assumptions when such data are missing or based on small samples. As such, the estimation of high-precision demographic parameters like age- or stage-specific survival and fertility rates should be a major aim of any study attempting to elucidate the mechanisms driving population decline and persistence.

The world's largest fish, the whale shark (*Rhincodon typus* Smith 1828), is also one of the least-studied and poorly understood shark species. No data on survival rates are available, and the reproductive data that do exist are based on extremely small sample sizes (Joung et al. 1996, Colman 1997). Even basic parameters such as growth, age at first reproduction, longevity, and population size are unknown for the majority of populations. However, some data exist for growth rates of captive juveniles (Chang et al. 1997), size and age at first reproduction (Pai et al. 1983, Satyanarayana Rao 1986, Wintner 2000), size distributions (Pravin 2000, Meekan et al. 2006), and abundance estimates for particular aggregations (Heyman et al. 2001, Meekan et al. 2006).

The predictable aggregation of whale sharks that occurs each year from March to June at Ningaloo Reef, Western Australia (Taylor 1996, Wilson et al. 2001a) has been the site of a large and lucrative eco-tourism industry where extensive photo-identification has been done over the last 15 years (Meekan et al. 2006). Recent studies have examined the potential to identify individuals over time using automated (Arzoumanian et al. 2005) or manual (Meekan et al. 2006) approaches, with the mark-resight data used to predict the size of the super-population participating in the Ningaloo aggregation at 300 to 500 individuals (Meekan et al. 2006). The photo-identification dataset can also be used within a capture-mark-recapture (CMR) modelling framework to estimate demographic parameters such as survival and capture probability.

Good estimates of whale shark demographic rates are essential components for assessing their conservation status. The species is listed as vulnerable according to World Conservation Union criteria (IUCN 2005) based on its rarity and reduction in catch rates in the regions where they are fished to supply meat throughout Asia (CITES 2002, IUCN 2005). Satellite tagging studies have verified that whale sharks attending the Ningaloo aggregation regularly migrate into Southeast Asian waters (Wilson et al. 2006; J. Polovina *et al.*, unpubl. data), with anecdotal evidence suggesting that some tagged animals have fallen victim to fishing in this region (J. Polovina *et al.*, unpubl. data). Additionally, Meekan *et al.* (2006) reported a decline in the proportion of large whale sharks seen between 1992 and 2004, which may indicate human-mediated changes in the age-class distribution of this population.

In this study we use the photo-identification database described in Meekan *et al.* (2006) to estimate apparent survival and capture probabilities for the Ningaloo Reef aggregation. We assess variation in survival over time, between the sexes, and as a function of an individual's total length. These survival estimates and other available demographic data reported in the literature are then incorporated into a series of age-classified Leslie matrix population models to assess the long-term persistence probability of the aggregation. Our overall aim is to provide a heuristic assessment of the possible population trajectory given our mark-recapture estimates of survival probability for this aggregation. This general template can be used to derive information on population assessments when demographic, abundance, and other key data are missing for species of conservation concern.

4.3.2 *Materials and Methods*

4.3.2.1 Study area and population

Our study was done at Ningaloo Reef (21° 32.4' S, 114° 6.0' E) off the coast of Exmouth in Western Australia from 1992 to 2004. Whale sharks aggregate predictably here from March to June each year (Taylor 1996, Wilson et al. 2001a) and their presence supports a highly profitable ecotourism industry (Davis et al. 1997, Davis 1998). Observers have taken photographs of sharks attending this aggregation for over 12 years for the purposes of photo-identification (Arzoumanian et al. 2005, Meekan et al. 2006).

4.3.2.2 Data collection

A total of 581 photographs were taken of whale sharks between March and July from 1992 to 2004 (Meekan et al. 2006). Photographs were made using an underwater still camera or digital video camera while snorkelling with the animal. Still images of sharks were captured from videotape for analysis. Total length (TL - tip of snout to end of caudal fin) and dorsal fin height (DIH) were recorded using a measuring tape after animals were photographed. In cases where only DIH was measured, we used a previously established equation to predict TL (Meekan et al. 2006):

$$TL = 1.059 + 10.348 DIH$$

Animal gender was determined whenever possible by distinguishing males based on the presence of claspers on the pelvic fins (Taylor 1994a). It was often difficult to discern claspers in relatively small (< 4 m TL) sharks, so those animals were recorded as indeterminate gender (Meekan et al. 2006).

4.3.2.3 Mark-recapture analysis

We used Cormack-Jolly-Seber (CJS) capture-mark-recapture (CMR) models (Cormack 1964, Jolly 1965, Seber 1970) implemented in program MARK (White & Burnham 1999) to model apparent survival (ϕ) and recapture (resighting) probability (p) of whale sharks participating in the Ningaloo Reef aggregation. Our primary interest was to estimate mean survival probability for inclusion into models projecting the population through time, so we endeavoured to assess variation in this parameter due to time and size effects. Estimates of ϕ within a CMR framework confound mortality with permanent emigration from the population, so some underlying knowledge of population closure is required to assess the degree of potential bias associated with survival estimates. We established previously that closed and open population models provided similar estimates of population size at the Ningaloo aggregation (Meekan et al. 2006). This suggests that the super-population is comprised of individuals that are not infrequent transients, but are those that attend the aggregation at least semi-regularly. As such, we expect that the estimates of survival derived from the CMR provided reasonable parameters for inclusion into population models.

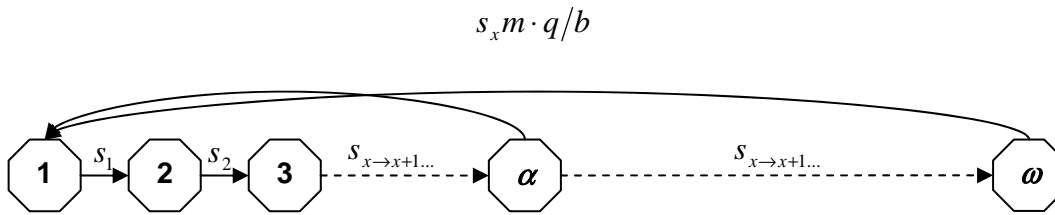
Our first analysis ignored the effects of size and sex and examined whether there was evidence for annual variation in ϕ and p over the course of the study (1992 – 2004). Models were compared using an information-theoretic measure of model parsimony, Akaike's Information Criterion (Akaike 1973, White & Burnham 1999) and goodness-of-fit was assessed using the simulation procedures provided in program MARK (White & Burnham 1999). A second model set was constructed to incorporate the effects of sex and time (16 models considered). Two separate analyses were done to determine whether there was a size- (length-) bias in survival using the estimates of total length. The first model set considered *size* as a categorical variable, where sharks < 8 m were considered immature and those \geq 8 m as mature (Colman 1997; see also below). This size-based grouping was applied only to the apparent survival parameter, with full time dependency considered for ϕ and p (16 models). A potentially more sensitive assessment of the effects of size on survival used total length as a standardized covariate in a linear model to predict the logit of ϕ (again, with the *time* effect considered for both ϕ and p). Here we examined the effects of total length as potentially altering both the intercept and slope of the linear model predicting $\logit(\phi)$ (12 models considered).

4.3.2.4 Population models

To examine how our estimated survival probabilities altered population projections, we constructed a series of age-based Leslie matrix population models to examine the potential population trajectory (Caswell et al. 1999). Although we have now estimated many of the demographic rates necessary to parameterize population models such as population size, sex ratio, size distribution (Meekan et al. 2006) and survival (this study), many other parameters are unknown or based on few data. As such, we defined several model scenarios that examined different assumptions with respect to the least-known parameters.

4.3.2.5 Model structure

Although stage-classified models have been used to project shark populations through time (Frisk et al. 2002, Mollet & Cailliet 2002, Otway et al. 2004), the relatively simple life history of elasmobranchs (i.e., sharks, rays and skates) coupled with the distorted elasticity patterns derived from stage-classified models (Mollet & Cailliet 2003b) argue for the use of simpler age-classified Leslie matrix models for whale sharks. We constructed a simple, deterministic and density-independent Leslie matrix (birth-pulse, post-breeding design – Caswell et al. 1999) for each of the model scenarios (described below) using the *R* package (R Core Development Team 2004) where the matrices were based on the general life cycle graph:



Here, s = the age-specific survival probability, x = age in years, α = the age at primiparity, ω = maximum age in years (longevity), m = litter size per female, q = pup sex ratio, and b = adult female reproduction frequency. For biennial reproduction, we calculated the discounted fertilities for every second year after α (i.e., setting the non-breeding years' discounted fertilities to 0).

4.3.2.6 Parameter estimates and assumptions

Whale sharks are live-bearers with an aplacental viviparous mode of development (Joung et al. 1996, Colman 1997). However, there is only one record of a captured female measuring approximately 11 m TL found to contain 300 embryos (Joung et al. 1996). There is no information available for the frequency of reproduction, with annual, biennial, and possibly more infrequent reproduction possible. As such, the fertility parameter was calculated as the number of potential pups (m) \times the assumed pup sex ratio (q) \div the frequency of reproduction (b) taking values of one or two (see Model Scenarios below).

Age at sexual maturity for females is thought to occur at $> 8 - 9$ m total length based on two female specimens of this size captured in Indian waters found to have immature ovaries (Pai et al. 1983, Satyanarayana Rao 1986). Colman (Colman 1997) therefore suggested that sexual maturity is reached at > 9 m. We assumed that all individuals ≥ 8 m were mature given the observed peak in the distribution of whale sharks at Ningaloo was 8 m (Meekan et al. 2006), which suggests an appearance in the seasonal aggregation of a particular (potentially) reproductive class relative to immatures. Additionally, growth rates (and hence length at sexual maturity) may be lower for animals regularly visiting the relatively cooler waters of Western Australia compared to India. Thus, based on our sample of individuals for which total length was known or estimated, the proportion of individuals that were mature (≥ 8 m) was $31 \div 108 = 0.29$. However, a study of vertebral growth rings from stranded individuals recovered in South Africa (Wintner 2000) suggested that an immature 5.77 m (TL) female was 22 years old assuming annual growth rings (age not validated), although maturity could not be determined absolutely given the lack of mature animals to autopsy. Nonetheless, we repeated all model scenarios where the duration of the immature stage was doubled (i.e., 24 years). No modification was made to overall longevity (see below) given that so few individuals remained after maximum age as to make little difference to the matrix outputs.

We used the von Bertalanffy growth function (von Bertalanffy 1938):

$$L_t = L_\infty - (L_\infty - L_0)e^{-kt}$$

where L_t = predicted total length (m) at age t (in years), L_∞ = asymptotic maximum length,
 L_0 = length at birth and k = a rate constant in units of reciprocal time.

This growth equation has been shown to be suitable for many elasmobranch species (Aasen 1963, Cailliet et al. 1992, Van Dykhuizen & Mollet 1992, Gallucci et al. 2006) and it can be used as a means to translate size-based estimates of survival to age-based probabilities and to estimate longevity. Pauly (2002) suggested that the rate constant (k) for whale sharks was 0.031 year^{-1} with a corresponding longevity > 100 years. This gives a first-year growth of 0.39 m, a value Pauly (2002) considered to be too large. The observed growth rate of young whale sharks in captivity was 0.81 m over 120 days (corresponding to 2.46 m annual growth) (Chang et al. 1997). We speculated and assumed that first-year growth in the wild was 0.80 (approximately twice that of Pauly 2002 and one third the captive rate), yielding a von Bertalanffy rate constant $k = 0.0637 \text{ year}^{-1}$. Using a birth length (L_0) of 0.58 m (Joung et al. 1996), maximum length (L_∞) = 13.7 (Compagno 1984) and assuming that maturity is reached at 8 m, this predicts age at maturity is approximately 13.0 years. Using a projected longevity of $5 \log_e 2/k = 54$ years (Ricker 1979), which in this case equates to an individual achieving 97 % of L_∞ , the duration of each stage is therefore 1 year for stage 1, 12 years for stage 2 (non-reproductive) and 41 years for stage 3 (reproductive). Finally, we set first-year survival to 0.5 based on the observed range of 0.38 – 0.65 for lemon sharks (*Negaprion brevirostris*; Gruber et al. 2001) and 0.37 – 0.82 for neonate black-tip sharks (*Carcharhinus limbatus*; Heupel & Simpfendorfer 2002). The paucity of juvenile survival data for almost all shark species prevents a more rigorous application of an evidence-based survival rate; however, we contend that given the balance of evidence, a first-year survival rate of 0.5 is a realistic mean for the heuristic purposes of inferring potential population trends.

The following sections outline various combinations of parameters and model assumptions to investigate the potential population trajectory using information derived from the CMR survival estimates. Model scenarios consider increasingly complex combinations of parameters under a deterministic framework only.

Model Scenario 1: In this scenario we constructed a simple deterministic model incorporating the mean survival estimate from the CMR models described above. Here, we maintained the first-year survival rate at 0.5 and applied the mean CMR survival rate to the remaining age classes regardless of reproductive status (non-reproductive or reproductive). We assumed a maximum invariant litter size of 300 (Joung et al. 1996) and two reproduction frequencies: annual and biennial. No density-dependent feedback mechanisms were implemented. Finally, this deterministic scenario considered both short (12 years) and long (24 years) non-reproductive stage durations.

Model Scenario 2: In this deterministic scenario we set the survival for the non-reproductive ages (years 1 to 12) to the mean probability of survival derived from the linear prediction based on total length over the size classes found at the Ningaloo Reef aggregation (4 to < 8 m). The reproductive female ages (13+) survival rate was likewise estimated as the mean survival for the size classes considered to be reproductive at Ningaloo (8 to 10 m). All other parameters and assumptions were maintained as in Scenario 1. Both short and long non-reproductive stage durations were examined.

Model Scenario 3: This deterministic matrix included an incrementing survival up to the age of 13 years, after which time survival was held constant. Age-specific survival probabilities were calculated from combination of the total length, survival and von Bertalanffy growth relationships described above. Short and long non-reproductive stage durations were considered separately, as well as annual and biennial reproduction frequencies.

Model Scenario 4: This matrix included incrementing survival up to the age of 25 years, with both non-reproductive stage durations considered separately and annual and biennial reproduction frequencies.

4.3.2.7 Elasticities of λ to changes in matrix parameters

For each deterministic base matrix, we identified the most important demographic parameters influencing the rate of population change. This type of perturbation analysis is achieved by calculating the sensitivity of the dominant eigenvalue of a matrix to changes in its elements, where the sensitivity of matrix element a_{ij} is the local slope of λ as a function of a_{ij} (Caswell et al. 1999). Elasticities (proportional sensitivities) were calculated for each matrix entry (survival, fertility) and summed to provide total elasticities for non-reproductive ($E(s_{nr})$) and reproductive female survival ($E(s_r)$), and adult fecundity ($E(m)$). This process requires taking into account the discounted fertilities (because survival is included in the first-row matrix entries in a post-breeding design) and then normalizing the elasticities for non-reproductive females, reproductive females and fertility so that they sum to 1 (Mollet & Cailliet 2003b). We also calculated the mean age of reproducing females at the stable age distribution (\bar{A}) for each matrix considered:

$$\bar{A} = \langle w, v \rangle$$

where w = left eigenvector of the matrix (age structure) and v = right eigenvector (reproductive values) when $w_1 = v_1 = 1$ (Mollet & Cailliet 2003b). Elasticities can then be calculated from \bar{A} (Mollet & Cailliet 2003b):

$$\begin{aligned} E(m) &= 1/(\bar{A} + 1) \\ E(s_{nr}) &= (\alpha)/(\bar{A} + 1) \\ E(s_r) &= (\bar{A} - \alpha)/(\bar{A} + 1) \end{aligned}$$

In the case of biennial reproduction frequency, elasticities must be calculated differently because the projection interval does not agree with the

reproductive cycle (Mollet & Cailliet 2003b). Following the formulae in Appendix 1(b) of Mollet & Cailliet (2003b), \bar{A} is adjusted to $\bar{A}/2$ (i.e., in 2-year units), α becomes $(\alpha + 1)/2$.

4.3.3 Results

4.3.3.1 Survival and capture probabilities

The base CJS analysis estimating apparent survival (ϕ) and capture probability (p) using data from 111 individual sharks demonstrated the saturated model (time-variant ϕ and p) fit the data reasonably well (probability of observing the model deviance as large = 0.464 based on 1000 iterations). Therefore, no adjustment to the AIC scores for over-dispersion (\hat{c}) was required (White & Burnham 1999). The most parsimonious model had time-invariant ϕ and p (Table 4.6); however, there was some evidence for time variation in both parameters based on AIC weights (Table 4.6). The null model gave an apparent annual survival of 0.825 (SE = 0.042; 95 % CI: 0.727 – 0.893; CV = 5.1 %) and capture probability of 0.184 (SE = 0.038; 95 % CI: 0.121 – 0.271; CV = 20.7 %). The model-averaged annual estimates of ϕ are shown in Table 4.7 (range: 0.737 – 0.890).

4.3.3.2 Sex differences in survival

There were 100 individuals of known sex in the database (81 males, 19 females). The saturated model with a sex effect in survival and capture probability fit the data reasonably well (probability of observing the model deviance as large = 0.969 based on 1000 iterations). However, the top five models accounting for over 97 % of the AIC weight had only a *time* effect on survival and no sex effect, suggesting that there were no survival differences between the sexes. There was some support for a sex effect on capture probability ($\phi(t) p(\text{sex})$ model with AIC weight = 21.4 %), but the model-averaged capture probability ranges for each sex overlapped (0.229 – 0.263 and 0.232 – 0.266 for males and females, respectively). As such, any possible sex bias in survival and recapture probabilities was ignored.

Table 4.6. Model ranking of Cormack-Jolly-Seber mark-recapture models estimating apparent survival (ϕ) and recapture probability (p) for whale sharks participating in the Ningaloo Reef (Western Australia) aggregation from 1992 to 2004. Shown are the delta Akaike's Information Criteria (ΔAIC), the AIC weight (AICwt), the number of parameters and the deviance for each model. A '(.)' denotes an invariant parameter, and '(t)' denotes a time-variant parameter.

Model	ΔAIC	AICwt	Parameters	Deviance
$\phi(.) p(.)$	0.00	0.588	2	53.459
$\phi(t) p(.)$	1.56	0.269	7	44.289
$\phi(.) p(t)$	3.07	0.126	7	45.800
$\phi(t) p(t)$	7.11	0.017	10	43.015

Table 4.7. Time-variant model-averaged estimates of apparent survival ($\hat{\phi}$) derived using Cormack-Jolly-Seber (CJS) mark-recapture models for whale sharks participating in the Ningaloo Reef (Western Australia) aggregation from 1992 to 2004. Also shown are the standard error (SE), unconditional SE and 95 % confidence interval for each model-averaged estimate.

Interval	$\hat{\phi}$	SE	Uncond SE	95 % CI
1992-1993	0.890	0.038	0.092	0.563 – 0.981
1993-1994	0.890	0.038	0.092	0.563 – 0.981
1994-1995	0.737	0.080	0.176	0.321 – 0.943
1995-1996	0.863	0.124	0.139	0.386 – 0.984
1996-2003 (annual)	0.842	0.056	0.064	0.676 – 0.931
2003-2004	0.773	-	-	-

4.3.3.3 Size differences in survival

There were size (total length) data for 75 individuals in the database (48 immature, 27 mature). Mean total length was 7.2 m and ranged from 4.4 to 9.7 m. In the size-class analysis, the saturated model fit the data reasonably well, although there was moderate evidence for a lack of fit to the data (probability of observing the model deviance as large = 0.052 based on 1000 iterations). The top 4 models (accounting for over 93 % of the AIC weight) had only a time effect on survival, suggesting no support for size (categorical) differences in survival.

The analysis using standardized total length as a covariate in the models demonstrated however, that there was a size bias in survival probability. The top four models all included a *length* and *time* effect on ϕ and accounted for over 92 % of the AIC weight. The most parsimonious model (AIC weight = 38 %) indicated a common intercept and time-variant slopes for the *length* effect on survival, but the second model had identical weight (38 %) and indicated both intercept and slopes were time-variant. Many of the parameters in the time-variant models were not estimable, so we chose to express the simpler relationship between length and ϕ by ignoring the *time* effect. The linear model derived was:

$$\text{logit}(\hat{\phi}) = 0.966 + 0.388 \left(\frac{TL - \overline{TL}}{\hat{\sigma}_{TL}} \right)$$

where TL is the estimated length of a whale shark, \overline{TL} is the mean total length of all sharks in the sample (7.2 m) and $\hat{\sigma}_{TL}$ is the standard deviation of total length from the sample (1.4 m). Thus, ignoring the effects of time, a 5 m shark has a predicted survival probability of 0.59 and a 9 m shark has predicted survival probability of 0.81.

4.3.3.4 Population models

The results of the Leslie matrix projection models are presented in Table 4.8 (age at first reproduction, α = 13 years) and Table 4.9 (α = 25 years). Of the 16 model combinations considered, 10 (63 %) indicated a decreasing population ($\lambda < 1$). For models based on α = 13, the mean age of reproducing females at the stable age distribution (\bar{A}) ranged from 15 to 23 years (Table 4.8), which increased to 29 to 37 years when α was increased 25 (Table 4.9). In all model combinations considered, the stable age distribution indicated a minority of reproductive females, but the dominance of first-year sharks or non-reproductive females varied according to particular combinations of vital rates and model assumptions. However, when survival rate was allowed to vary with age (length), the number of first-year sharks dominated the stable age distribution. All scenarios had higher total elasticities for non-reproductive female survival ($E(s_{nr})$) compared to that for reproductive female survival ($E(s_r)$) (Tables 4.8 and 4.9). $E(m)$ was inferior to $E(s_{nr})$ and $E(s_r)$ in all cases.

Table 4.8. Matrix parameters calculated for each Model Scenario considered when age at first reproduction (α) = 13, for both annual and biennial reproduction frequencies. Shown are the dominant eigenvalue of the deterministic matrix (λ), the stable stage distribution (SSD) for first-year (0 to 1 year), juvenile (1 to 12 years) and adult (13 to 54 years) sharks, respectively, the mean age of reproducing females at the stable stage distribution (\bar{A}), the combined elasticities for non-reproductive ($E(s_{nr})$) and reproductive ($E(s_r)$) survival, the ratio of elasticities for reproductive to non-reproductive survival ($E(s_r)/E(s_{nr})$) and the elasticity for fertility ($E(m)$).

Scenario	Description	λ	SSD	\bar{A}	$E(s_{nr})$	$E(s_r)$	$E(s_r)/E(s_{nr})$	$E(m)$	
<u>Annual</u>									
reproduction									
Scenario 1	constant survival	1.2658	0.47, 0.53, 0.005	14.87	0.8191	0.1179	0.1440	0.0630	
Scenario 2	average length-based survival	1.0438	0.45, 0.54, 0.004	16.53	0.7412	0.2013	0.2713	0.0571	
Scenario 3	length-based survival to age 13	0.9500	0.60, 0.40, 0.005	17.12	0.7173	0.2275	0.3171	0.0552	
Scenario 4	length-based survival to age 25	0.9751	0.61, 0.39, 0.005	20.61	0.6015	0.3522	0.5855	0.0463	
<u>Biennial</u>									
reproduction									
Scenario 1	constant survival	1.2229	0.44, 0.55, 0.007	14.67	0.7798	0.1002	0.1285	0.1200	
Scenario 2	average length-based survival	1.0078	0.43, 0.57, 0.006	16.73	0.6940	0.1992	0.2870	0.1068	
Scenario 3	length-based survival to age 13	0.9177	0.58, 0.42, 0.008	17.52	0.6658	0.2317	0.3480	0.1024	
Scenario 4	length-based survival to age 25	0.9470	0.59, 0.40, 0.008	22.38	0.5332	0.3848	0.7218	0.0820	

Table 4.9. Matrix parameters calculated for each Model Scenario considered when age at first reproduction (α) = 25, for both annual and biennial reproduction frequencies. Shown are the dominant eigenvalue of the deterministic matrix (λ), the stable stage distribution (SSD) for first-year (0 to 1 year), juvenile (1 to 24 years) and adult (25 to 54 years) sharks, respectively, the mean age of reproducing females at the stable stage distribution (\bar{A}), the combined elasticities for non-reproductive ($E(s_{nr})$) and reproductive ($E(s_r)$) survival, the ratio of elasticities for reproductive to non-reproductive survival ($E(s_r)/E(s_{nr})$) and the elasticity for fertility ($E(m)$).

Scenario	Description	λ	SSD	\bar{A}	$E(s_{nr})$	$E(s_r)$	$E(s_{nr})/E(s_r)$	$E(m)$	
<u>Annual</u>									
reproduction									
Scenario 1	constant survival	1.0508	0.31, 0.69, 0.003	28.63	0.8436	0.1223	0.1453	0.0337	
Scenario 2	average length-based survival	0.9432	0.38, 0.62, 0.003	30.91	0.7836	0.1851	0.2362	0.0313	
Scenario 3	length-based survival to age 13	0.8715	0.54, 0.44, 0.004	31.56	0.7679	0.2014	0.2623	0.0307	
Scenario 4	length-based survival to age 25	0.9352	0.58, 0.41, 0.004	35.45	0.6859	0.2867	0.4180	0.0274	
<u>Biennial</u>									
reproduction									
Scenario 1	constant survival	1.0295	0.29, 0.71, 0.004	28.55	0.8183	0.1162	0.1420	0.0655	
Scenario 2	average length-based survival	0.9244	0.36, 0.63, 0.005	31.20	0.7531	0.1867	0.2479	0.0602	
Scenario 3	length-based survival to age 13	0.8542	0.53, 0.47, 0.007	31.95	0.7364	0.2047	0.2780	0.0589	
Scenario 4	length-based survival to age 25	0.9178	0.57, 0.42, 0.008	36.23	0.6540	0.2937	0.4491	0.0523	

4.3.4 Discussion

The paucity of data describing the variation in vital rates in species of conservation concern is a common problem for ecological modellers (Boyce 1992, Morris & Doak 2002). Indeed, obtaining estimates of vital rates and their corresponding variances may be difficult or impossible for many species, especially for long-lived marine vertebrates (Caughley 1994, Heppell et al. 2000). As such, generalizations for predicting population persistence derived from few data or based on allometric or species-specific ecological characteristics are often sought (Beissinger & Westphal 1998, Belovsky et al. 2004, Brook et al. 2006). Although heuristically useful (Brook et al. 2002), matrix population models lacking quantitatively derived vital rates are subject to many assumptions that are difficult to test or validate. In the case of the relatively poorly studied whale shark, we have provided the first estimates of survival rates based on mark-recapture data. These estimates, combined within a series of deterministic Leslie matrix models have permitted the first quantitative appraisal of the projected long-term trends of this vulnerable population.

Although caution must be exercised in interpreting our population matrices (see below), the variants of the age-classified Leslie matrix models using different estimates of non-reproductive female and reproductive female survival and stage duration demonstrate the importance of considering biologically plausible covariates in survival analyses, especially for long-lived and slow-growing species. For example, ignoring the important effect of total length (size) on estimates of survival led to the conclusion of population increase (i.e., $\lambda > 1$) regardless of changes to age at first reproduction and frequency of reproduction. However, when we used the more parsimonious information-theoretic model predictions of length-varying survival, the importance of stage duration became much more apparent. With the shorter stage duration and age-specific survival estimates, most scenarios predicted a declining population ($\lambda < 1$), and doubling the interval between reproductive events resulted in an increased rate of decline.

Many elasmobranchs have a reproductive cycle of two years (Cortés 2002), and a few species breed more infrequently, every three years (Mollet et al. 2000, Cortés 2002). Although the reproduction interval of whale sharks is currently unknown, the precautionary principle for fisheries management (Caddy & Mahon 1995) suggests that assuming annual reproduction would be inappropriate for whale sharks. Reducing the breeding frequency further to once every three years, the estimates of λ under the most realistic Scenario 4 (length-based survival to age 25) are further depressed to 0.9325 (age at first breeding = 13) and 0.9077 (age at first breeding = 25). Despite the severe lack of demographic data for this species (especially with respect to its reproductive capacity), the models that incorporated the most biologically realistic parameter estimates and assumptions support the conclusion of a declining population visiting Ningaloo Reef each year. However, this conclusion depends on some as yet untested assumptions. The duration of the non-reproductive stage and lifespan of the species are important determinants in the projections using length-varying estimates of survival. Of these two

parameters, perhaps it is more tractable to collect information on growth rates that would verify the onset of reproduction.

The super-population of whale sharks participating in the Ningaloo Reef aggregation has been estimated at 300 – 500 individuals of which approximately 16 % were identified as female (74 % male and 10 % indeterminate gender) (Meekan et al. 2006). It should also be noted that pups and yearlings have never been observed at Ningaloo Reef, so pup production is likely to occur elsewhere. It is unknown whether the female component of the Ningaloo aggregation represents a small proportion of females that normally participate in a larger, sexually segregated female population that has yet to be identified. If there is an important sexual segregation of whale sharks as has been documented for other elasmobranch species (Springer 1967, Klimley 1987, Sims et al. 2001, Sims 2006), then the small number of females observed at Ningaloo might not necessarily comprise the majority of the reproductively active females contributing new individuals to the aggregation. The embryo and juvenile sex ratio of many shark species does not depart from unity (Joung & Chen 1995, Chen et al. 1997b, Liu et al. 1999, Smale & Goosen 1999, Joung et al. 2005, Hazin et al. 2006), and Beckley *et al.* (1997) reported an equal sex ratio for stranded, immature whale sharks in South Africa. As such, we expect the low percentage (16 %) of females at Ningaloo to be the result of sexual segregation, perhaps with many females within the super-population instead spending their time farther north in Southeast Asian waters (Theberge & Dearden 2006), around the Indian coastline (Satyanarayana Rao 1986), or even in the vicinity of the Galápagos Islands (Stewart & Wilson 2005).

Our analyses also revealed some important aspects of the contribution of length- (and age-) specific survival rates to population rates of change. Elasticities from a mean matrix cannot by themselves accurately predict how λ fluctuates with variation in vital rates because of non-equality of change in these parameters, non-linearities in their relationships to λ , and differences in the coefficients of variation among matrix elements (Mills et al. 1999, Stewart & Wilson 2005). Additionally, the reported elasticities were derived from deterministic matrices, which can be poor predictors of stochastic elasticities when the environment is extremely variable or includes catastrophic mortality events (Benton & Grant 1996). Although it has been shown previously that whale shark numbers at Ningaloo Reef fluctuate in response to environmental events such as El Niño-Southern Oscillation (ENSO; Wilson et al. 2001a), we deliberately avoided using stochastic projections given the uncertainty associated with mean values of reproductive output, reproduction frequency and age at first reproduction.

With these caveats in mind, we found that the highest elasticities were for immature (i.e., non-reproductive) survival rates. This result agrees with re-assessments of elasticities for most elasmobranch species (Mollet & Cailliet 2002, 2003b). Even though others have suggested that elasmobranch population rates of change are more sensitive to adult (reproductive) survival (Colman 1997, Smith et al. 1998, Walker 1998, Frisk et al. 2001, Cortés 2002), the elasticities for many stage-classified models are calculated inappropriately

(see Mollet & Cailliet 2003b). When calculated correctly (and more easily) using age-classified Leslie matrix models, we found that immature female survival was a far more important determinant of the potential population rate of change for whale sharks; therefore, estimating this parameter precisely should be a prime area of research.

The limitation of producing robust estimates of the reproductive potential of whale sharks is problematic and may ultimately prevent the construction of reliable population viability analyses. There have only been nine 'juveniles' (0.55 – 0.93 total length) recorded for whale sharks (Colman 1997), some of which have been found in the stomach of other oceanic predators (blue shark, *Prionace glauca* and blue marlin, *Makaira mazara*) (Kukuyev 1996, Colman 1997). Neither have there ever been reports of individuals between 0.93 and 3.00 m total length, suggesting that there are either extremely high predation rates on small individuals, or that reproduction occurs in the open ocean and is so dispersed that the probability of detecting young individuals is too low to quantify precisely. Another potential limitation is the likely density-related changes in vital rates used to parameterize the models, especially considering the pervasiveness of density dependence in nature (Brook & Bradshaw 2006). We deliberately avoided constructing hypothetical density-dependent relationships in our simple scenarios given the complete lack of associated data, but we acknowledge that persistence predictions and parameter elasticities are likely to vary with the inclusion of density dependence (Grant & Benton 2000, Drake 2005). However, future work on this aggregation and other whale shark populations should attempt to assess the degree to which vital rates are modified by density fluctuations. This may be achieved perhaps initially by examining the evidence for density dependence in phenomenological time series of relative abundance (e.g., sightings-per-unit-effort data; Brook & Bradshaw 2006).

Our analyses beg the questions – (1) what is the state of the Ningaloo Reef whale shark population and (2) can our analyses shed light on its persistence probability? Recent evidence from Ningaloo suggests that the population is comprised of a larger proportion of juveniles compared to previous decades (Meekan et al. 2006). However, severe declines have not been reported, so we believe that the real population trajectory lies somewhere between the extremes of our predictions. Additionally, an aggregation of juvenile whale sharks in nearby Thailand has recently declined by 96 % (sightings per unit effort from 1992 to 2001) (Theberge & Dearden 2006). These observations, in combination with our results, lend credence to the hypothesis that the regional (Australasian) population of whale sharks is declining. As such, our results have several conservation implications for this and other large oceanic shark species. The wide dispersal range and sensitivity of population growth rates to minor variation in survival makes this species particularly vulnerable to anthropogenic sources of mortality (customary and commercial fishing). Non-reproductive whale sharks aggregating at Ningaloo travel long distances (1000s km) to Southeast Asian waters (Wilson et al. 2006) where they are potentially susceptible to fishing pressure (Eckert et al. 2002; Polovina et al. unpubl. data). The low population size (300 – 500 individuals; Meekan et al. 2006), the possibility of limited mixing (Wilson et al. 2006; Polovina et al. unpubl. data), and the high elasticity of λ to non-

reproductive female survival rates demonstrate the need for concerted conservation efforts to span national boundaries (Wilson et al. 2006).

The collection of mark-recapture databases for whale sharks has provided the first quantitative foundation for testing hypotheses regarding population persistence in one of the largest known aggregations of this species. Continued development of this database will be important for adjusting the predictions of matrix-based models, and will also provide a template for other large, oceanic marine vertebrates for which few demographic data exist. Our combination of standard CJS mark-recapture estimates of apparent survival and age-classified Leslie matrix models allowed us to assess the biological reality of the demographic rate estimates for whale sharks. In so doing, our study has highlighted the demographic processes that conservation practitioners should aim to maximize to increase the persistence probability of this, and other large elasmobranch species.

4.4 SCARRING PATTERNS AND RELATIVE MORTALITY RATES OF INDIAN OCEAN WHALE SHARKS

4.4.1 Introduction

Declines in populations of whale sharks (*Rhincodon typus*) have been observed and predicted in many regions (CITES 2002, IUCN 2005, Theberge & Dearden 2006, Bradshaw et al. 2007, Bradshaw et al. In press). This species, the world's largest fish and one of the most wide-ranging marine vertebrates (Wilson et al. 2006, Bradshaw et al. 2007, Castro et al. 2007), is known to be susceptible to a variety of mortality sources including direct harvest, ecosystem modification and collisions with ocean-going vessels (Bradshaw et al. 2007) that may be the cause of these declines. The prospect of losing such a large and iconic species is of both conservation and economic concern. For example, the disappearance of the species could precipitate annual losses in the order of US\$47.5 million generated from whale shark tourism globally (Graham 2004).

Although potential sources of population decline have been recognised for many years (Colman 1997), their relative importance remains largely unquantified. The large size (> 12 m total length), slow swimming speeds (between 1 and 3 km·h⁻¹) (Gunn et al. 1999, Eckert & Stewart 2001, Eckert et al. 2002, Hsu et al. 2007) and tendency to spend a large proportion of their time at the surface (Wilson et al. 2006) renders this species particularly vulnerable to ramming by vessels (Gudger 1940), artisanal and commercial fishing (Colman 1997) and predation by large sharks and some cetaceans (Fitzpatrick et al. 2006). Additionally, these animals make annual long-distance migrations through international and national waters (Wilson et al. 2006). This means that whale sharks may experience protection by legislation and management in some areas, while being exploited in other parts of their range (Bradshaw et al. In press), a problem common to other wide ranging marine species such as

North Atlantic right whales (*Eubalaena glacialis*) (Ward-Geiger et al. 2005). Thus, identifying mortality sources and areas where these pose a risk to whale sharks are important steps in formulating global initiatives for conservation.

Legal and illegal fishing of whale sharks is often suggested to be a central driver of population declines (Chen & Phipps 2002, CITES 2002, Bradshaw et al. 2007). This mortality is relatively easy to quantify because animals are brought to shore by fishermen and sold in markets. However, other factors such as predation and boat strike may be equally important, but are far more difficult to estimate reliably because they are thought to occur principally in the open ocean. Despite the lack of direct observation, where whale sharks survive predatory attacks or collisions with ships, some evidence of these events may be left in the form of scars or injuries on the body. Analysis of scarring patterns may thus provide an insight into the relative importance and source of mortality afflicting whale sharks, as is the case for other large marine species such as manta rays, manatees, whales, dolphins and seals (e.g., Kraus 1990, Hiruki et al. 1993, Angliss & DeMaster 1997, Heithaus 2001b, Laist et al. 2001, Naessig & Lanyon 2004, Rommel et al. 2007).

Each whale shark has a unique pattern of spots and stripes (Meekan et al. 2006) that can be used to identify individuals (Speed et al. 2007). Photographic databases are now used worldwide in mark-recapture studies to document population trends and estimate demographic rates (Fujiwara & Caswell 2001, Stevick et al. 2001, Bradshaw et al. 2003, Meekan et al. 2006, Speed et al. 2007). A combination of information on rates and source of scarring in conjunction with mark-recapture data may provide a means to quantify relative mortality rates among whale shark populations experiencing different direct and indirect human impacts. Similar analyses of the survival implications of scarring and injuries have been made in other taxa (e.g., Iberian lynx *Lynx pardinus*, North Atlantic right whale *Eubalaena glacialis*, Hawaiian monk seals *Monachus schauinslandi* – Kraus 1990, Garcia-Perea 2000); however, no study to date has combined photo-identification with scarring to test the hypothesis that scarring is indicative of higher mortality rates.

This study documents the severity, positioning and likely causes of scars observed on whale sharks participating in three Indian Ocean aggregations: 1) Ningaloo Reef, western Australia, 2) Mahe, Seychelles and 3) southern Mozambique. Using capture-mark-recapture (CMR) models and quantified scarring patterns, relative apparent survival rates were estimated between two of the study sites (Ningaloo and Seychelles) and compared to shipping traffic rates to estimate the potential high risk boat-strike areas for this species.

4.4.2 Materials and methods

4.4.2.1 Scarring databases and image matching

Scarring image libraries were constructed from larger whale shark photo-identification databases for Ningaloo Reef, western Australia (22° 50' S, 113° 40' E), Maher, Seychelles (4°6' S, 55° 26' E) and southern Mozambique (23° 52' S, 35°

33° E). (Fig. 4.12). The Ningaloo scarring library consisted of images of individuals with scars taken over 10 capture sessions (years) between 1992 and 2006 (not including 1997-2000 and 2002). The Seychelles library consisted of images taken over 6 capture sessions between 2001 and 2006 and also included scarring information obtained from a tagging database. The Mozambique scarring library consisted of images taken during one capture session over the 2004/2005 season.

Images were matched using the software I³S (Van Tienhoven et al. 2007b) and visual confirmation following guidelines for use on whale sharks outlined in Speed *et al.* (2007). Where images did not lend themselves to the fingerprinting process required for I³S, images were matched manually by an experienced photo-archivist (Meekan et al. 2006) using not only the pattern of natural pigmentation, but also other individually unique identifiers such as scars and tags.

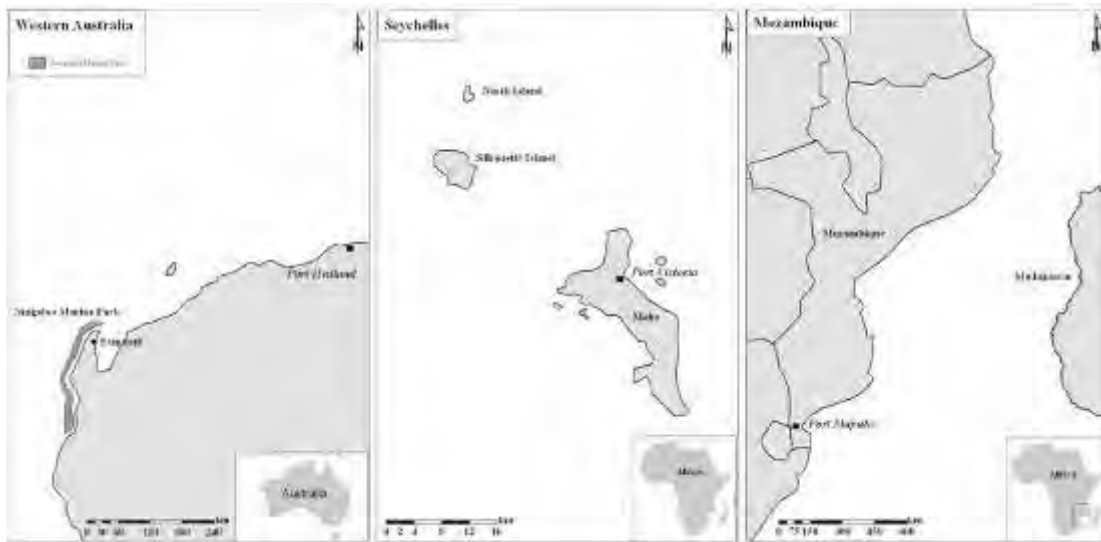


Figure 4.12. Indian Ocean whale shark aggregation sites – Ningaloo Reef (Western Australia), Seychelles and Mozambique.

4.4.2.2 Scarring categories

Seven scarring categories were created based on images present in the libraries for each region: (1) abrasions, (2) lacerations, (3) nicks, (4) bites, (5) blunt trauma, (6) amputations and (7) 'other' (Appendix 1). Each image was assigned to one or more of the seven categories by visual inspection. The severity of scarring was classified into two groups: 'major' or 'minor'. Major scars were considered to be potentially life-threatening and included complete or near-complete amputation of the first dorsal, pectoral or caudal fins, lacerations penetrating the sub-dermal layer, blunt trauma around the head or gills and large shark bites (> 30 cm in length) (Fig. 4.13A - C). Minor scars were considered to be superficial and included abrasions, partial amputations, small bites, nicks, and 'other' (Fig. 4.13D - F).

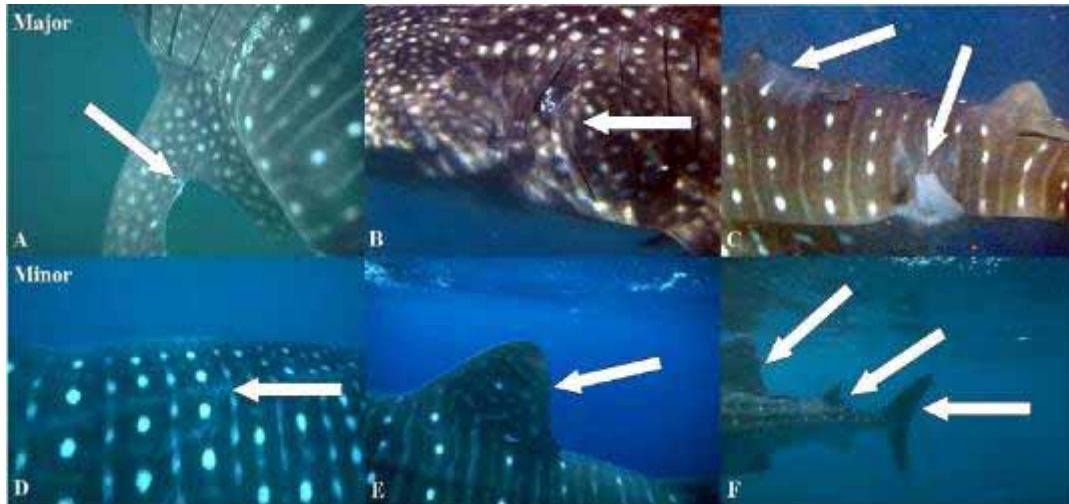


Figure 4.13. Classification of scar severity. Images A – C show examples of ‘major’ scarring; A) (Photo© G. Taylor) A large bite taken out of the left pectoral fin, B) (Photo© A. Richards) Blunt trauma to the left side of head and C) (Photo© A. Richards) Bites taken out of dorsal fin and left flank. Images D – F (Photos© G. Taylor) show examples of ‘minor’ scarring; D) Abrasion on the right flank, E) Small nick taken out of the trailing edge of the dorsal fin and F) Nicks and small bites taken out of the first and second dorsal fins and caudal fin.

4.4.2.3 Database comparisons

The frequency of individuals with scars per capture session was initially calculated for each database and then combined to give total numbers of scarred individuals per aggregation. Due to differing numbers of sample periods among databases, estimates were standardised for cross-database comparisons by dividing the number of scarred individuals by the total number of individuals photographed for each aggregation. The total number of sharks scarred per database was also recalculated with the scarring categories ‘nicks’ and ‘abrasion’ omitted for two reasons: (1) the scar categories are unlikely to affect survival rates given that they are by definition superficial wounds, and (2) minor scars were often not photographed on individuals at Ningaloo Reef. The proportion of individuals with differing scar types were calculated for each aggregation (with minor scars omitted). A randomised multinomial contingency analysis (10000 iterations) was constructed to test the hypothesis that the distribution of animals in each scar category differed among aggregations. Scar categories were combined into three main classes to avoid low-frequency classes dominating results: bites, blunt trauma, and lacerations/amputation (ignoring other categories). Scar positions on the body of each shark were also recorded to compare among aggregations and to determine the most commonly scarred areas of the body.

4.4.2.4 Effects of scarring on apparent survival

Capture histories consisting of inter-season resights from Ningaloo and Seychelles were initially constructed using matches identified by I³S as well as tags deployed in Seychelles. The capture history for the Mozambique aggregation was unable to be included because there were too few sample sessions. To avoid double-counting, individuals with only the left side

photographed were removed from the Ningaloo capture history (because there were fewer left-side photographs than right-side), while individuals with only the right side photographed were removed from the Seychelles capture history (fewer right-side photographs there) (Meekan et al. 2006). Capture histories included (1) whether the individual was scarred or not (three categories: major, minor and none), (2) the putative source of scarring (anthropogenic, bite, unknown, none) and (3) the body position of the scar (fin, body or none). Cormack-Jolly-Seber (CJS) CMR models were used and executed in the program MARK (White & Burnham 1999) to model apparent survival of (ϕ) and resighting probability (p) (Bradshaw et al. 2007). The major focus of this analysis was to assess whether the apparent survival rate for whale sharks with scars differed from whale sharks without scars.

The initial analysis examined whether there was evidence for time variance in ϕ or p over the study period (1992-2006) at Ningaloo, which was analogous to the approach adopted by Bradshaw *et al.* (2007), although the current analysis included two additional capture sessions (2005 & 2006). This process was then repeated for the Seychelles aggregation. The second analysis included scarring as an additional group effect on ϕ or p . Scar type and severity were examined to assess whether they influenced ϕ or p . Models were compared using Akaike's Information Criterion corrected for small sample sizes (AIC_c) (Burnham & Anderson 2002) and goodness-of-fit was estimated using the bootstrap GOF function in program MARK (White & Burnham 1999).

4.4.2.5 Shipping activity around aggregations

Due to limited availability of spatial shipping data for the east coast of Africa, shipping density was unable to be modelled around the three whale shark aggregations. Consequently, the number of commercial ships (i.e., container ships and bulk carriers) calling in at the largest and nearest port to each aggregation was obtained through associated port authorities as a proxy for shipping intensity. Where available, statistics on smaller vessel traffic were also noted. Ship-calling data were obtained for the fiscal year from 01 July 2005 through to 30 June 2006 from Port Hedland (Australia), Port Victoria (Seychelles) and Port Maputo (Mozambique) authorities.

4.4.3 Results

The Seychelles aggregation had the highest percentage of scarred individuals (67 %, 534 of 797), followed by Mozambique (37.2 %, 67 of 180) and Ningaloo (27 %, 84 of 311). After the removal of minor scars (nicks and abrasions), the total percentages of scarred individuals per aggregation dropped to 45.3 % (361 of 797) for Seychelles, 22.7 % (41 of 180) for Mozambique, and 20 % (62 of 311) for Ningaloo Reef.

Nicks were the most abundant scar category in all aggregations (Table 4.10). After the removal of these minor scars (nicks and abrasions), bites were the most common scars (Table 4.10; Fig. 4.14).

Table 4.10. Percentage of individuals within scar type and body location category among three Indian Ocean aggregations observed.

	Aggregation		
	Ningaloo	Seychelles	Mozambique
Scar Type (%)			
abrasions	21.4	14.6	40.3
lacerations	8.3	34.5	7.5
nicks	11.9	48.6	14.9
bites	44.0	21.4	14.9
blunt trauma	8.3	5.1	7.5
amputations	15.5	21.4	26.9
other	2.4	4.4	10.4
Scar Location (%)			
head	9.5	11.6	30
dorsal fin	30.0	38.5	20.9
caudal fin	25.0	62.2	31.3
pectoral fin	22.6	14.4	22.4
flank	25.0	25.2	34.3

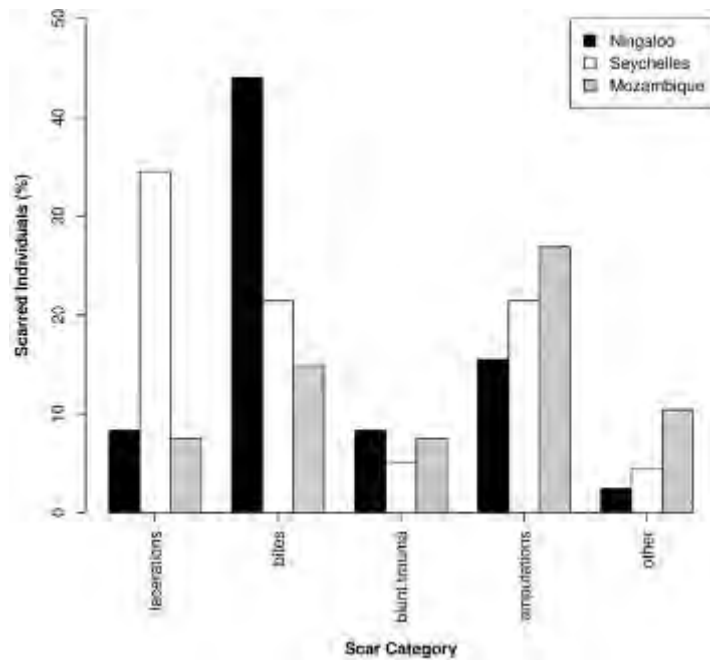


Figure 4.14. Percentage occurrence of individuals within scar categories by location.

The randomised contingency analysis demonstrated that the probability of generating the same among-site differences in the distribution of individuals within the three major scar categories (bites, blunt trauma, lacerations/amputations) was = 0.0007 (based on 10000 iterations). Observed and expected frequencies were similar for Seychelles and Mozambique animals, but Ningaloo had more bites and fewer amputations/lacerations than expected (Fig. 4.15). Caudal fins were the most commonly scarred body part (Fig. 4.16A) at all locations (Fig. 4.16B).

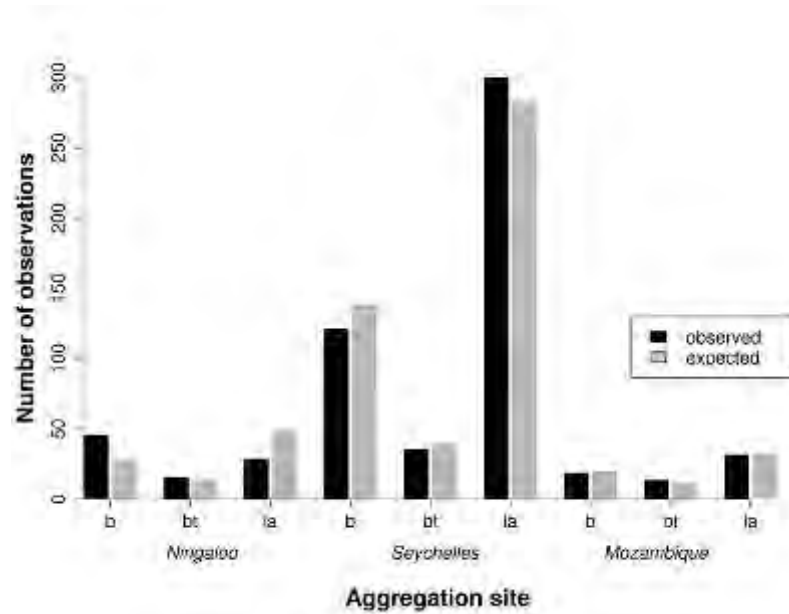


Figure 4.15. Observed and expected numbers of sharks in each scarring category among aggregation sites. *b = bites, bt = blunt trauma and la = lacerations and amputations.

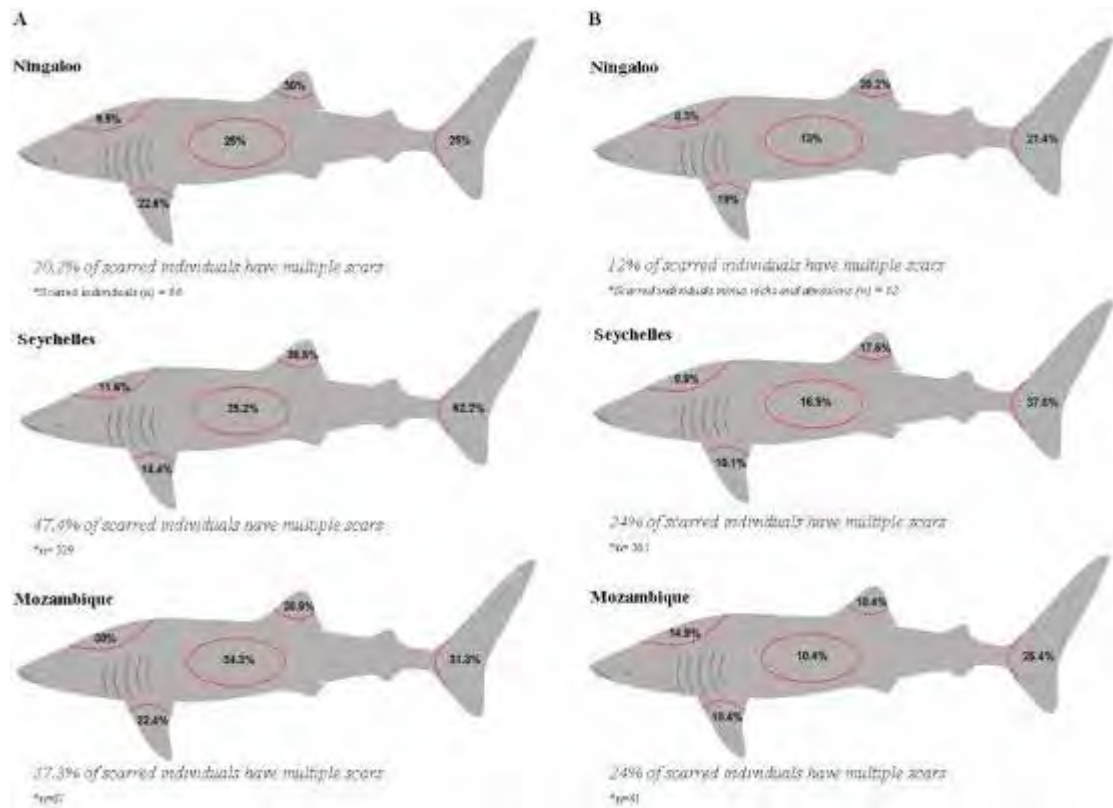


Figure 4.16. A) Position of scars on body by aggregation site B) Position of scars on body by aggregation site (nicks and abrasions omitted).

The saturated Cormack-Jolly-Seber capture-mark-recapture model $\phi(t^*s) p(t^*s)$ relating time (t) and scarring (s) to apparent survival (ϕ) and resight probability (p) for the 221 individual sharks seen at Ningaloo fit the data reasonably well (probability of observing the model deviance as large = 0.134 based on 1000 iterations). Therefore, no adjustment to AIC_c was made for over-dispersion (White & Burnham 1999). Most parameters were inestimable using the t^*s interaction for ϕ and p , so these group factors were considered separately in all subsequent model comparisons. The most highly ranked model ($wAIC_c = 0.84$) had scar effects on apparent survival and time-variant resighting probability $\phi(s) p(t)$ (Table 4.11); however, confidence intervals for scarred and not-scarred individuals overlapped substantially (Table 4.11).

There was no over-dispersion detected for the Seychelles dataset, and the most highly ranked model ($wAIC_c = 0.99$) demonstrated time variance in ϕ and p (Table 4.11). However, many of the interval estimates of ϕ were inestimable, so the second-most highly ranked model was used to test for scarring effects. Again, there was considerable overlap in the confidence intervals between scarred and non-scarred individuals (Table 4.12), suggesting little evidence for an effect on apparent survival. Apparent survival rates were considerably lower in the Seychelles (~ 0.50) compared to Ningaloo Reef (~ 0.90).

Table 4.11. Five most highly ranked Cormack-Jolly-Seber models testing the effects of scarring (s) and time (t) on apparent survival (ϕ) and resight probability (p) of whale sharks participating in the Ningaloo Reef aggregation between 1992 and 2006, and at Seychelles between 2001 and 2006. Shown are the difference in Akaike's Information Criterion corrected for small sample sizes between the current and top-ranked model (ΔAIC_c), AIC_c weight ($wAIC_c$), the number of model parameters (k), and model deviance. '(.)' indicates a constant parameter.

Model	ΔAIC_c	$wAIC_c$	k	Deviance
Ningaloo Reef				
$\phi(s)p(t)$	0.000	0.842	10	133.021
$\phi(.)p(t)$	3.381	0.155	10	136.402
$\phi(.)p(.)$	58.406	0.000	2	208.329
$\phi(t)p(.)$	58.114	0.000	10	191.135
$\phi(t)p(t)$	12.535	0.000	17	129.777
Seychelles				
$\phi(t)p(t)$	0.000	0.999	8	31.894
$\phi(s)p(t)$	25.201	0.000	7	61.233
$\phi(.)p(t)$	23.491	0.000	6	61.580
$\phi(.)p(.)$	57.842	0.000	2	104.074
$\phi(t)p(.)$	28.918	0.000	6	67.006

Table 4.12. Apparent survival estimates for whale sharks with and without scarring at Ningaloo Reef and Seychelles based on Cormack-Jolly-Seber mark-recapture models.

Model		ϕ	SE	Lower 95 % CI	Upper 95 % CI
Ningaloo Reef					
$\phi(s)p(t)$	<i>Not Scarred</i>	0.858	0.033	0.781	0.911
	<i>Scarred</i>	0.929	0.033	0.830	0.972
Seychelles					
$\phi(s)p(t)$	<i>Not Scarred</i>	0.502	0.060	0.386	0.618
	<i>Scarred</i>	0.538	0.070	0.402	0.669

ϕ = apparent survival, s = scarred or not, p = sighting probability, t = time.

The number of commercial ships that called in to Port Hedland during the fiscal year of 2005/2006 was 925 (excluding fishing vessels). The intended destinations after departure for the majority of these ships were Asia. The number of commercial vessels calling in to Port Victoria during the same period was 510;

however, there was also a notably high number of fishing vessels (628), both purse-seine and long-line, whose next destination was the high seas. For commercial vessels, the next port of call was largely South East African and Indian Ocean island ports or European or Asian ports. The number of commercial ships that docked at Port Maputo during this period was 674, with the final destination of most of these vessels also being Asia.

4.4.4 Discussion

The prevalence and origin of large scars on whale sharks leads to the hypothesis that activities other than direct over-exploitation from fishing may also contribute to observed and modelled population declines of whale sharks in the Indian Ocean. Of the 1288 individuals identified in this study, 36 % bore prominent scars (i.e., excluding nicks and abrasions). Bite marks were the most common form of major scar (27 % of scarred individuals) followed by lacerations/amputations (19 %) and blunt trauma (7 %). Bite scars were probably the result of attacks by large predators such as sharks and killer whales. Non-lethal attacks by a large (> 4 m) predatory shark on a whale shark have been recorded at Ningaloo Reef (Fitzpatrick et al. 2006) and a fatal attack on an 8-m whale shark by killer whales (*Orcinus orca*) was observed in the Gulf of California (O'Sullivan & Mitchell 2000). None of the bite scars found on whale sharks in this study could be unambiguously attributed to killer whales, as virtually all were healed wounds that lacked the distinctive teeth rake marks that are definitive of attacks by these predators (Naessig & Lanyon 2004).

Many whale sharks bore the evidence of collisions with boats and this phenomenon was probably responsible for the majority of lacerations, amputations and blunt trauma injuries. The parallel rows of deep lacerations found on the backs of many sharks were clear evidence of strikes by ship propellers (Rommel et al. 2007), while the large blunt trauma injuries on the head and flanks of sharks were probably mostly due to ramming by ship bows (Laist et al. 2001). In the case of amputations, some of these injuries may have also have been due to predatory attacks, albeit most could be distinguished from ship strike by the circular edge of the wound (see Fig. 4.13A).

Ramming of whale sharks by ocean-going vessels was well-recognised as a threat to whale sharks in the early years of the 20th century (Gudger 1940), but such deaths of sharks are rarely recorded today. Due to relatively thin sub-dermal fat layers, whale shark carcasses may sink quickly in comparison to whales (Ward-Geiger et al. 2005) so that most mortalities due to collisions probably go unnoticed (Stevens 2007). However, boat collisions are likely still to reduce the survival probability of whale sharks, particularly since shipping traffic along coasts and in the open oceans has more than tripled since the 1940s (Lloyd's Register of Shipping 1939-2005), and today's cargo vessels are larger and travel at much greater speeds. Mortalities due to shipping have been recorded in recent times; for example, a whale shark was struck and killed by a large vessel off the coast of the Seychelles in 2000 (Fig. 4.16). Other possible evidence of ship strikes comes from Pop-up Archival Tag (PSAT; Wilson et al. 2006) deployments on whale sharks at Ningaloo Reef. These tags are designed to release and float to the surface once an animal remains at a constant

depth and temperature for more than two days. During one deployment, a 4-m whale shark travelling at the surface along the Northwest Shelf, one of Australia's busiest shipping routes, suddenly descended to 900 m and remained there for 12 hours (Wilson et al. 2006). Given diving records of other animals and the water temperature at that depth (2°C) this behaviour may represent mortality due to a ship strike, although other causes (e.g., predatory attacks) cannot be excluded.

The proportion of sharks bearing predator bite scars and those with laceration/amputation and blunt trauma scars were similar (27 versus 26% of individuals, respectively). However, this does not necessarily mean that they translated into a similar number of deaths. Lacerations and blunt trauma scars generally appeared more severe than bite scars because the former covered larger areas of the body and in the case of lacerations, propellers often left multiple scars on the same animal. Furthermore, bite scars tended to be most common on the fins, and evidence from Ningaloo suggests that animals can recover from even total fin amputation by bites (Fitzpatrick et al. 2006). Thus, ship collisions may be responsible for greater mortalities of whale sharks, even if rates of scarring from this source are similar to bites.

Although minor scars (nicks and abrasions) are unlikely to alter individual survival probability, they may act as warning signs of other threats. Three of the Mozambique sharks possessed abrasions similar to those described from net-entangled cetaceans (Angliss & DeMaster 1997). Tuna purse-seine fisheries in the western Indian Ocean catch small numbers of whale sharks (Romanov 1998), while gill-net fisheries also occasionally catch whale sharks (Stevens 2007). Five Mozambique sharks had minor abrasions or lacerations characteristic of small boat propeller strikes (Rommel et al. 2007). Similar scars have been noted at other aggregation sites (Graham & Roberts 2007, Rowat et al. 2007) and in some cases, were possibly caused by vessels used to view sharks (Rowat et al. 2007). 'Go-slow' areas within aggregation sites, already used for some other slow-moving marine species (Laist & Shaw 2006) and regulated through the whale shark code of conduct in Western Australia, may reduce the probability and severity of ship strikes.

The caudal fin was the area most commonly scarred. This is not surprising, given that these animals spend most of their lives in < 100 m of water and much time swimming at the surface (Wilson et al. 2006). For this reason, the caudal fin will be the body part most likely to be struck by a boat. The caudal fin may also be an attractive target for predators because it may be easier to grip with teeth and sever in contrast to the body trunk (Long & Jones 1996).

Whale sharks at Ningaloo Reef had more bites (44 % of individuals) and fewer lacerations and blunt trauma scars than those at either the Seychelles or Mozambique. Although this suggests that there may be higher rates of predation at Ningaloo and lower numbers of boat strikes, it needs to be recognised that these animals are highly migratory (Eckert & Stewart 2001, Eckert et al. 2002, Rowat & Gore 2006, Wilson et al. 2006) and that the healed scars observed at the study sites may have been accrued in distant parts of their range. Despite the incongruence of shipping activity and relative scarring

rates among sites (e.g., there were more commercial vessels near Ningaloo despite a lower incidence of ship-related injuries), there is some evidence that small boat traffic at Ningaloo may be lower than at either the Seychelles or Mozambique. Ningaloo Reef is largely protected by an expansive marine park in a remote area of Western Australia, whereas the coastal areas around Mozambique and Seychelles are heavily populated and have a strong fishing presence. Furthermore, tiger sharks (*Galeocerdo cuvier*) and other large species of requiem (Carcharhinidae) sharks (Fitzpatrick et al. 2006) are regularly sighted by spotter planes during the peak whale shark season at Ningaloo Reef, and are also temporarily abundant in other areas immediately to the south such as Shark Bay (Heithaus 2001a). In contrast, large, predatory sharks are rarely spotted during aerial surveys during whale shark season in the Seychelles (D. Rowat, unpubl. data).

The hypothesis that observed rates of scarring were indicative of relative mortality rates at two widely separated aggregations on opposite sides of the Indian Ocean experiencing different intensities of shipping traffic was not supported. The lack of a scarring effect on apparent survival may indicate that individuals surviving ship strike and predator attack are no more susceptible to premature mortality than their unscathed counterparts, but the relative contribution of different shipping rates to explain regional variance in survival patterns still cannot be ruled out. Despite the observation there appears to be fewer commercial vessels around whale shark aggregation sites in the western Indian Ocean (Seychelles and Mozambique), large fishing vessels may still pose threats to whale sharks in this region. Whale shark mortalities related to ship-strikes from commercial and fishing vessel may contribute to the lower apparent survival rates observed in the Seychelles; however, better and longer-term mark-recapture data are required to confirm this. Indeed, even individuals with major scarring returned repeatedly to their aggregation sites, indicating that scarring itself is unlikely to alter survival or migration patterns. Whether scars are naturally or anthropogenically derived, whale sharks appear to be resistant to the hypothetical negative effects of injuries on survival, but may still demonstrate reductions in maturation time or reproductive ability (Hiruki et al. 1993).

It must also be assumed that estimates of apparent survival between the Ningaloo and Seychelles aggregations are comparable based on equal probabilities of permanent emigration. Capture histories analysed in the Cormack-Jolly-Seber framework provide estimates of apparent survival that are confounded with permanent emigration (White & Burnham 1999), so a higher proportion of transients in one population will bias apparent survival estimates downward. Nonetheless, the large difference in apparent survival between Ningaloo and Seychelles is suggestive of true differences in survival rates and requires longer-term data to verify this adequately.

This analysis of three Indian Ocean whale shark populations based on photo-identification provided little evidence that major or minor scarring affects survival rates, despite the prevalence of injuries and scarring among the individuals examined. However, the magnitude of shipping-related deaths remains unquantified and may only be revealed with dedicated large-ship

surveys near known aggregation sites. Due to their apparent resilience to scarring, it is true that whale sharks may not fear shark, man or ship; however, current trends in population status suggest they are not as impervious to these threats as previously thought.

